Electronic Research Archive

http://www.aimspress.com/journal/era

ERA, 33(4): 2246–2274.
DOI: 10.3934/era.2025098
Received: 18 January 2025
Revised: 11 March 2025
Accepted: 25 March 2025
Published: 16 April 2025

Research article

Non-destructive test method of wood moisture content based on multiple varying bounds integral numerical method

Cui Guo[1,*], Yixue Wang[1], Haibin Wang[2], Xiongbo Zheng[1] and Bin Zhao[3]

[1] College of Mathematical Sciences, Harbin Engineering University, Harbin 150001, China
[2] College of Mechanical and Electrical Engineering, Northeast Forestry University, Harbin 150040, China
[3] College of Power and Energy Engineering, Harbin Engineering University, Harbin 150001, China

* **Correspondence:** Email: 2185835@163.com.

Abstract: For the wood moisture content (MC) detection engineering problem by planar capacitive sensors, a high accuracy is required. To meet this demand, we constructed a mathematical model in this paper, as this is an inverse problem in the multi-physics fields. Furthermore, we proposed a new numerical method with high accuracy, which is called the multiple varying bounds integral method. We applied this numerical method to establish a high accuracy and compact numerical scheme for solving this model. Because the unknown function is continuous in some physical fields and discontinuous in others, we needed to use different numerical methods to construct numerical schemes in these fields. For example, we used the multiple varying bounds integral (MVBI) method and interpolation methods. Next, based on the results of the numerical experiments, a regression model was established between capacitance and the dielectric constant of wood. The results indicated that the larger the value of dielectric constant, the larger the value of capacitance. This is consistent with the physical principle. Moreover, the determination coefficient R^2 of the regression model was greater than 0.91. Additionally, the confidence degree exceeded 0.99, which implies that the reliability of the regression model is strong. This indicates that the regression model shows a high goodness of fit and high confidence degree.

Keywords: wood moisture content; multiple varying bounds integral numerical method; dielectric constant; regression analysis; mathematical model

Assumptions of the model and notation description

Some notations and basic assumptions are given in this paper:

1) B_1 and B_2 denote two thin electrode plates of the capacitive sensor.

2) B denotes the measured wood, and B, B_1, B_2 do not intersect each other.

3) $\varepsilon = \varepsilon(x, y, z)$ denotes the dielectric constant of the wood at the point (x, y, z).

4) $\tilde{\varepsilon}$ denotes the dielectric constant of air.

5) $V = V(x, y, z)$ denotes the potential at the point (x, y, z).

6) V_1 and V_2 denote the potentials of B_1 and B_2, respectively.

7) $E = E(x, y, z)$ denotes the electric field strength at the point (x, y, z).

8) C denotes the capacitance of the capacitive sensor.

9) q_1 and q_2 denote the charge carried by B_1 and B_2, respectively, with $q_1 = q_2$. Additionally, q_1 also satisfies

$$C = \frac{q_1}{V_1 - V_2}.$$

10) ∂B_{in} and ∂B_{out} denote the interior and exterior of the wood boundary, respectively.

1. Introduction

Wood moisture content (MC) detection is one essential problem in the modern world. All wood products contain some level of moisture, and too high or too low MC can cause quality issues in wood products. Thus, inaccurate MC detection severely impacts quality control in the wood processing industry. It also impacts the maintenance of wooden historical buildings and the protection of rare tree species [1–7]. Once wood products or wooden structures are completed, their shape and material no longer change. The key factors determining their internal quality are primarily the MC and drying stress. When the equilibrium moisture content is reached, cracking and deformation are least likely to occur. In recent years, inaccurate MC detection has resulted in a wood utilization rate of only 50%–60%. In contrast, technologically advanced countries have achieved rates as high as 90%. This has led to frequent significant economic losses in the national economy.

Due to the significant social and economic benefits of MC detection, scholars from various countries have conducted extensive and in-depth research on this topic. With continuous research, methods for MC detection [8] have also been continuously developed and improved. Martin et al. [9] used the resistance method to study the relationship between MC and average resistivity of silver fir. Van Blokland and Adamopoulos [10] analyzed the electrical resistance characteristics of Norway spruce. Through simple linear regression, they derived a first-order polynomial function relationship between MC and resistance of the wood. However, the resistance method can obtain only ideal measurement results when the MC is between 6% and 25%. The measurement error is severely limited by the value of MC. Edwards and Jarvis [11], Batranin et al. [12], and Penttila et al. [13] used the ray technique to detect changes in MC, which are not limited by specific MC values. However, the ray technique has high detection costs, slow speeds, and safety hazards, posing challenges for inspectors. Qin et al. [14] studied the relationship between MC and ε but noted that different tree species require different dielectric models. Compared to these methods, we aim to find a more widely applicable method that can meet more measurement requirements. Capacitive sensors [15] are electronic components that can convert the measured physical quantities and their

variation laws into capacitance and capacitance change laws. They have the outstanding advantage of performing non-contact, continuous, and high-precision measurements. Therefore, we consider measuring the capacitance between the electrode plates to calculate MC [16–19]. On the other hand, we found that most researchers use only experimental methods to MC detection. We propose combining experiments with mathematical methods to build a mathematical model and complete the MC detection.

For the mathematical model, it is also very important to choose the appropriate numerical method, which will have a great influence on numerical accuracy and speed. To some extent, the finite volume method [20–22] has absorbed some advantages of the finite element method and the finite difference method. The finite volume method is mainly applied to solve fluid flow and heat transfer problems. With this method, the numerical scheme obtained can keep some properties of original differential equations, such as the conservation of mass, momentum, and energy.

The multiple varying bounds integral method [23–27] is a new numerical method developed based on the finite volume method. First, by means of multiple integrals, all the derivatives in the space direction of the differential equation can be eliminated. In this way, the differential equation can be equitably represented by another new equation that contains only the unknown function than its derivatives. On this basis, we begin to construct the corresponding numerical scheme for this new equation. This avoids the occurrence of large errors greatly, especially where the change rate of the derivative is large. Furthermore, multiple integrals with varying bounds are important. Different Integral bounds can help us get different numerical schemes. Depending on the physical properties of differential equation, we can choose an appropriate scheme from them.

The layout of the paper is as follows. In Section 2, we provide the methodology for MC detection. In Section 3, we discuss the steps for MC detection. In Section 4, by multiple varying bounds integral method, we construct second-order compact discrete schemes in fields where the potential is continuous and discontinuous, respectively, and conduct error estimation and numerical experiments. In Section 5, a conclusion is provided.

2. Methodology for wood moisture content detection

A core issue for wood moisture content detection is to construct the function relationship between the capacitance C and the dielectric constant ε. The methodology is shown in Figure 1. This is a multi-physics inverse problem with partial differential equations. We choose many suitable values of ε. On this basis, through the mathematics model we constructed, we obtain the values of C. The data C and ε are regressed to fit a function $\varepsilon = \varepsilon(C)$. Then, by capacitive sensor, we measure the value of C, and substitute it into the aforementioned fitted function to calculate ε. Ultimately, by the one-to-one correspondence between ε and MC, we obtain the value of MC.

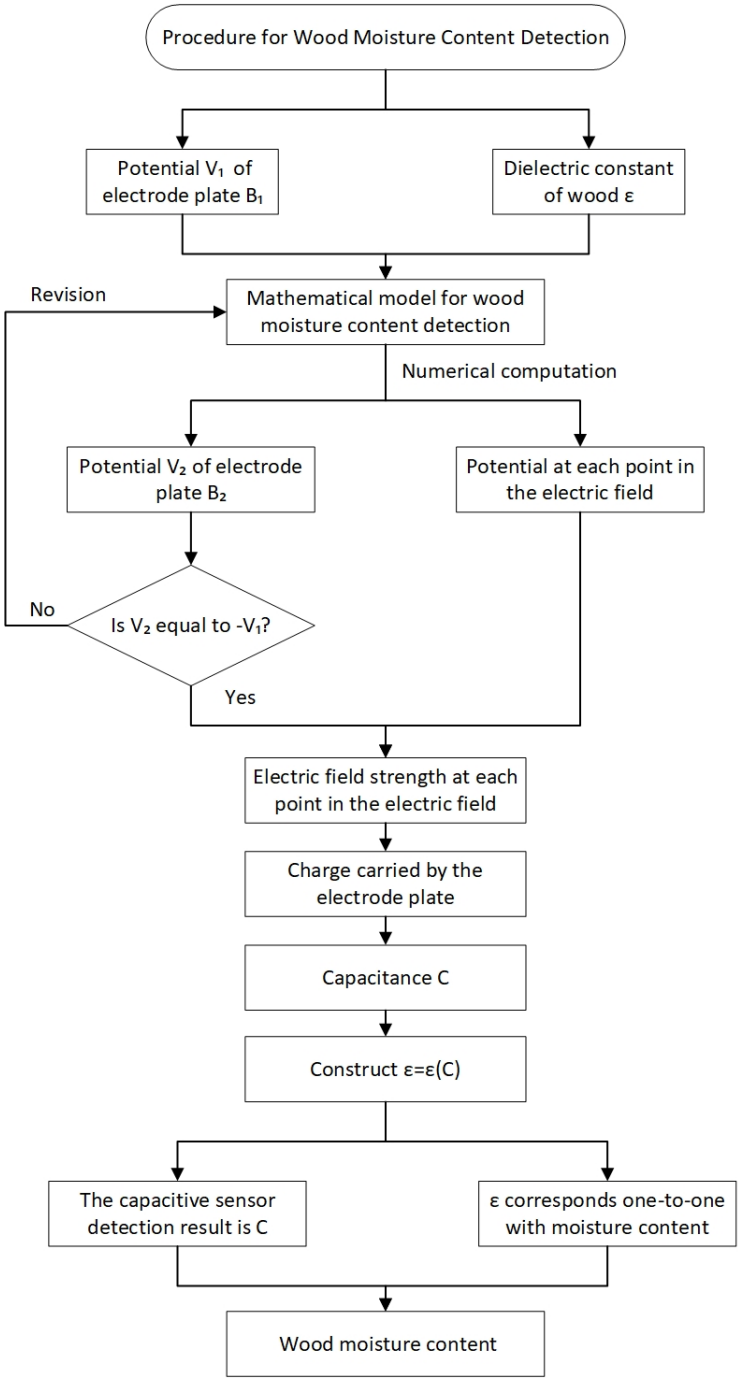

Figure 1. Methodology for wood moisture content detection.

3. Steps for wood MC detection

We focus on constructing the function relationship between ε and C. The steps are as follows:
1) The measured wood B and the electrode plates B_1 and B_2 are shown in Figure 2.

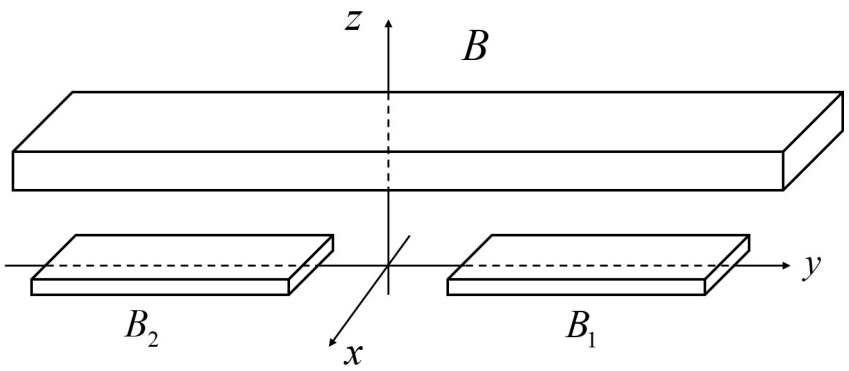

Figure 2. The placement of B, B_1, and B_2.

During practical wood detection, MC is always indirectly measured. This is accomplished by finding a physical quantity correlated with MC, measuring this quantity, and establishing its relationship with MC to determine MC. In this paper, we use the dielectric constant as the physical quantity related to MC.

As shown in Figure 2, two metal plates of identical material and specifications are used as the electrode plates of the capacitive sensor and are fixed at specific positions, labeled B_1 and B_2. According to physical law, the capacitive sensor's internal dielectric material affects the amount of charge it can store. Therefore, the capacitance between the two plates is influenced by the surrounding environment. If the surrounding environment remains unchanged, and the measured wood is placed on top of the plates, an electromagnetic field is generated around it. If the dimension of measured wood is known, the value of C will be uniquely determined by ε, establishing a one-to-one correspondence between C and ε. Thus, by measuring C, we can obtain ε. Additionally, we have found that there is a one-to-one relationship between ε and MC. Therefore, by ε as an intermediary, we first establish the relationship between C and ε, and then leverage the corresponding relationship between ε and MC to determine MC.

2) According to the mathematical model in [28], satisfied by the potential $V(x, y, z)$,

$$\begin{cases} \nabla^2 V(x,y,z) = 0, & (x,y,z) \in (R^3 - B_1 - B_2 - \overline{B}), \\ \tilde{\varepsilon} \iint_{\partial B_1} |gradV(x,y,z)|\, dS = -\tilde{\varepsilon} \iint_{\partial B_2} |gradV(x,y,z)|\, dS, \\ \varepsilon \left.\dfrac{\partial V(x,y,z)}{\partial n}\right|_{\partial B_{in}} = \tilde{\varepsilon} \left.\dfrac{\partial V(x,y,z)}{\partial n}\right|_{\partial B_{out}}, \\ V(x,y,z)\Big|_{\partial B_{in}} = V(x,y,z)\Big|_{\partial B_{out}}, \\ \lim\limits_{\sqrt{x^2+y^2+z^2}\to\infty} V(x,y,z) = 0. \end{cases} \tag{3.1}$$

If V_1 and ε are given, then $V = V(x, y, z)$ and V_2 are uniquely determined.

3) If $V(x, y, z)$ is determined, the electric field strength $E(x, y, z)$ can be determined by

$$E(x, y, z) = -gradV(x, y, z).$$

It can be seen that $E(x, y, z)$ is related to $\varepsilon(x, y, z)$.

4) By integral,

$$q_1 = \tilde{\varepsilon} \oiint_{\partial B_1} |gradV_1(x, y, z)| \, dS = \iint_{\partial B_1} \tilde{\varepsilon} E_1(x, y, z) dS,$$

and

$$q_2 = \tilde{\varepsilon} \oiint_{\partial B_2} |gradV_2(x, y, z)| \, dS = \iint_{\partial B_2} \tilde{\varepsilon} E_2(x, y, z) dS,$$

the charge q_1 (or q_2) of B_1 (or B_2) is obtained [29]. Obviously, q_1 (or q_2) is also related to $\varepsilon(x, y, z)$.

5) By the equation

$$C = \frac{q_1}{V_1 - V_2},$$

the capacitance C can be obtained, and it can be seen that C is also related to $\varepsilon(x, y, z)$.

Thus, $V(x, y, z)$, $E(x, y, z)$, and C are related to $\varepsilon(x, y, z)$. Therefore, when V_1 and ε are given, it means that the system is determined. In view of this, when we regard the values of ε as integers from 1 to 20, a series of corresponding C can be obtained. Through regression analysis, we can construct the function relationship between ε and C.

4. The multiple varying bounds integral method

To maintain the advantages of the finite volume method and meet the high-precision demands of detection problems, we develop a new method called the multiple varying bounds integral method to calculate the capacitive sensor model.

The two electrode plates occupy the domain

$$B_1 = \{(x, y, z) \, | \, -a \le x \le a, b \le y \le c, 0 \le z \le d\},$$

and

$$B_2 = \{(x, y, z) \, | \, -a \le x \le a, -b \le y \le -c, 0 \le z \le d\}.$$

The measured wood occupies the domain

$$B = \left\{(x, y, z) | \, -k \le x \le k, -l \le y \le l, m \le z \le n\right\}.$$

This is an unbounded problem. To achieve numerical computation, we set a reasonable artificial boundary $[x_L, x_R]\times[y_L, y_R]\times[z_L, z_R]$. The computational domain is discretized by taking $h_x = \frac{x_R - x_L}{N_x}$, $h_y = \frac{y_R - y_L}{N_y}$ and $h_z = \frac{z_R - z_L}{N_z}$ as the step size in the direction of the x-axis, y-axis, and z-axis, respectively. Here N_x, N_y, and N_z are three given positive integers, so we get $(N_x + 1) \times \left(N_y + 1\right) \times (N_z + 1)$ grid nodes. Let each grid node be (x_i, y_j, z_k), where $x_i = x_L + ih_x \, (i = 0, 1, \cdots, N_x), y_j = y_L + jh_y \left(j = 0, 1, \cdots, N_y\right)$ and $z_k = z_L + kh_z \, (k = 0, 1, \cdots, N_z)$. Set $V(x_i, y_j, z_k) = V_{i,j,k}$, which approximately represents the corresponding potential at each node.

4.1. Establishment of a compact discrete scheme

In fact, the mathematical model to be solved is a multi-physics inverse problem. Therefore, for different fields, we should select appropriate numerical methods for different differential equations. We divide physical fields into two regions: Field 1, where $V_{i,j,k}$ is continuous, and field 2, where $V_{i,j,k}$ is discontinuous.

4.1.1. Field 1

In the computational domain, the variable $V_{i,j,k}$ is continuous except at the faces, vertices and edges of the wood. Therefore, the multiple varying bounds integral method can be directly applied to discretize the equation in field 1.

When $(x, y, z) \in (R^3 - B_1 - B_2 - \overline{B})$, the potential $V(x, y, z)$ satisfies

$$\nabla^2 V(x, y, z) = 0, \tag{4.1}$$

and is continuous, so we can directly apply the multiple varying bounds integral method in this field to integrate Eq (4.1). We perform multiple varying bound integrals with respect to x, y, and z on both sides of Eq (4.1), so we have

$$\int_{z_1}^{z_2}\int_{y_1}^{y_2}\int_{x_1}^{x_2}(\frac{\partial^2 V}{\partial x^2}+\frac{\partial^2 V}{\partial y^2}+\frac{\partial^2 V}{\partial z^2})dxdydz = 0. \tag{4.2}$$

By Eq (4.2)

$$\int_{z_1}^{z_2}\int_{y_1}^{y_2}(\frac{\partial V}{\partial x_2}-\frac{\partial V}{\partial x_1})dydz+\int_{z_1}^{z_2}\int_{x_1}^{x_2}(\frac{\partial V}{\partial y_2}-\frac{\partial V}{\partial y_1})dxdz+\int_{y_1}^{y_2}\int_{x_1}^{x_2}(\frac{\partial V}{\partial z_2}-\frac{\partial V}{\partial z_1})dxdy = 0. \tag{4.3}$$

Then, integrating both sides of Eq (4.3) within the control volume, we have

$$\begin{aligned}&\int_{z_k-\alpha_z}^{z_k}\int_{z_k}^{z_k+\frac{\alpha_z}{2}}\int_{y_j-\alpha_y}^{y_j}\int_{y_j}^{y_j+\frac{\alpha_y}{2}}\int_{x_i-\alpha_x}^{x_i}\int_{x_i}^{x_i+\frac{\alpha_x}{2}}[\int_{z_1}^{z_2}\int_{y_1}^{y_2}(\frac{\partial V}{\partial x_2}-\frac{\partial V}{\partial x_1})dydz\\&+\int_{z_1}^{z_2}\int_{x_1}^{x_2}(\frac{\partial V}{\partial y_2}-\frac{\partial V}{\partial y_1})dxdz+\int_{y_1}^{y_2}\int_{x_1}^{x_2}(\frac{\partial V}{\partial z_2}-\frac{\partial V}{\partial z_1})dxdy]dx_1dx_2dy_1dy_2dz_1dz_2 = 0.\end{aligned} \tag{4.4}$$

The three terms on the left-hand side of Eq (4.4) have identical structures. Therefore, we compute only the first term on the left-hand side. The other two terms can be handled similarly.

$$\begin{aligned}&\int_{z_k-\alpha_z}^{z_k}\int_{z_k}^{z_k+\frac{\alpha_z}{2}}\int_{y_j-\alpha_y}^{y_j}\int_{y_j}^{y_j+\frac{\alpha_y}{2}}\int_{x_i-\alpha_x}^{x_i}\int_{x_i}^{x_i+\frac{\alpha_x}{2}}[\int_{z_1}^{z_2}\int_{y_1}^{y_2}(\frac{\partial V}{\partial x_2}-\frac{\partial V}{\partial x_1})dydz]dx_1dx_2dy_1dy_2dz_1dz_2\\&=\int_{z_k-\alpha_z}^{z_k}\int_{z_k}^{z_k+\frac{\alpha_z}{2}}\int_{y_j-\alpha_y}^{y_j}\int_{y_j}^{y_j+\frac{\alpha_y}{2}}\int_{z_1}^{z_2}\int_{y_1}^{y_2}[\int_{x_i-\alpha_x}^{x_i}\int_{x_i}^{x_i+\frac{\alpha_x}{2}}(\frac{\partial V}{\partial x_2}-\frac{\partial V}{\partial x_1})dx_1dx_2]dydzdy_1dy_2dz_1dz_2\\&=\int_{z_k-\alpha_z}^{z_k}\int_{z_k}^{z_k+\frac{\alpha_z}{2}}\int_{y_j-\alpha_y}^{y_j}\int_{y_j}^{y_j+\frac{\alpha_y}{2}}\int_{z_1}^{z_2}\int_{y_1}^{y_2}\{\alpha_x[V(x_i+\frac{\alpha_x}{2},y,z)-V(x_i,y,z)]\\&\qquad-\frac{\alpha_x}{2}[V(x_i,y,z)-V(x_i-\alpha_x,y,z)]\}dydzdy_1dy_2dz_1dz_2\\&=\int_{z_k-\alpha_z}^{z_k}\int_{z_k}^{z_k+\frac{\alpha_z}{2}}\int_{y_j-\alpha_y}^{y_j}\int_{y_j}^{y_j+\frac{\alpha_y}{2}}\int_{z_1}^{z_2}\int_{y_1}^{y_2}\{\alpha_x[V(x_i+\frac{\alpha_x}{2},y,z)-\frac{3}{2}V(x_i,y,z)\\&\qquad+\frac{1}{2}V(x_i-\alpha_x,y,z)]\}dydzdy_1dy_2dz_1dz_2,\end{aligned} \tag{4.5}$$

where, α_x, α_y and α_z are undetermined parameters. In the case of following the wood physical properties, we set $\alpha_x = \alpha_y = \alpha_z = \alpha$ and $h_x = h_y = h_z = h$.

Through the integral, the derivative function of an unknown function $V(x, y, z)$ can be eliminated, thus reducing numerical errors, especially where the rate of change of the derivative is large. Next, we interpolate the original function of $V(x, y, z)$. Here, let the node step size in each direction be h. We select three interpolation nodes in each of the x, y, and z directions, generating a total of 27 grid nodes (x_i, y_j, z_k), (x_i, y_{j-1}, z_k), (x_i, y_{j+1}, z_k), (x_{i-1}, y_j, z_k), (x_{i-1}, y_{j-1}, z_k), (x_{i-1}, y_{j+1}, z_k), (x_{i+1}, y_j, z_k), (x_{i+1}, y_{j-1}, z_k), (x_{i+1}, y_{j+1}, z_k), (x_i, y_j, z_{k-1}), (x_i, y_{j-1}, z_{k-1}), (x_i, y_{j+1}, z_{k-1}), (x_{i-1}, y_j, z_{k-1}), $(x_{i-1}, y_{j-1}, z_{k-1})$, $(x_{i-1}, y_{j+1}, z_{k-1})$, (x_{i+1}, y_j, z_{k-1}), $(x_{i+1}, y_{j-1}, z_{k-1})$, $(x_{i+1}, y_{j+1}, z_{k-1})$, (x_i, y_j, z_{k-2}), (x_i, y_{j-1}, z_{k-2}), (x_i, y_{j+1}, z_{k-2}), (x_{i-1}, y_j, z_{k-2}), $(x_{i-1}, y_{j-1}, z_{k-2})$, $(x_{i-1}, y_{j+1}, z_{k-2})$, (x_{i+1}, y_j, z_{k-2}), $(x_{i+1}, y_{j-1}, z_{k-2})$, $(x_{i+1}, y_{j+1}, z_{k-2})$, as shown in Figure 3.

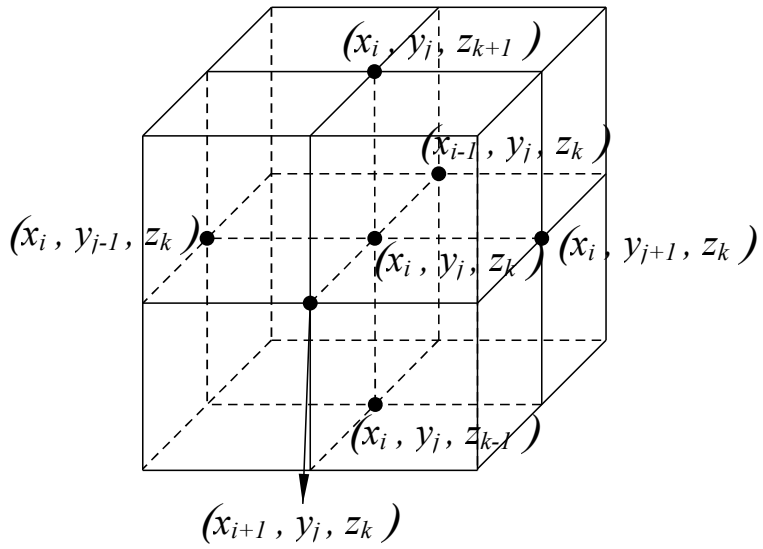

Figure 3. The interpolation nodes in field 1.

Based on these 27 nodes, we construct the interpolating function for the unknown function $V(x, y, z)$, as follows

$$V(x,y,z) = \sum_{m=i-1}^{i+1}\sum_{s=j-1}^{j+1}\sum_{t=k-1}^{k+1} V(x_m, y_s, z_t) \prod_{\substack{p=i-1\\p\neq m}}^{i+1} \frac{x-x_p}{x_m-x_p} \prod_{\substack{q=j-1\\q\neq s}}^{j+1} \frac{y-y_q}{y_s-y_q} \prod_{\substack{r=k-1\\r\neq t}}^{k+1} \frac{z-z_r}{z_t-z_r}. \tag{4.6}$$

Substituting Eq (4.6) into Eq (4.5), we have

$$\begin{aligned}
&\lambda_1 V_{i-1,j-1,k-1} - 2\lambda_1 V_{i,j-1,k-1} + \lambda_1 V_{i+1,j-1,k-1} + \lambda_2 V_{i-1,j,k-1} - 2\lambda_2 V_{i,j,k-1} + \lambda_2 V_{i+1,j,k-1}\\
&+ \lambda_3 V_{i-1,j+1,k-1} - 2\lambda_3 V_{i,j+1,k-1} + \lambda_3 V_{i+1,j+1,k-1} + \lambda_2 V_{i-1,j-1,k} - 2\lambda_2 V_{i,j-1,k} + \lambda_2 V_{i+1,j-1}\\
&+ \lambda_4 V_{i-1,j,k} - 2\lambda_4 V_{i,j,k} + \lambda_4 V_{i+1,j,k} + \lambda_5 V_{i-1,j+1,k} - 2\lambda_5 V_{i,j+1,k} + \lambda_5 V_{i+1,j+1,k}\\
&+ \lambda_3 V_{i-1,j-1,k+1} - 2\lambda_3 V_{i,j-1,k+1} + \lambda_3 V_{i+1,j-1,k+1} + \lambda_5 V_{i-1,j,k+1} - 2\lambda_5 V_{i,j,k+1} + \lambda_5 V_{i+1,j,k+1}\\
&+ \lambda_6 V_{i-1,j+1,k+1} - 2\lambda_6 V_{i,j+1,k+1} + \lambda_6 V_{i+1,j+1,k+1} = 0,
\end{aligned} \tag{4.7}$$

where $\lambda_1 = \frac{\alpha^2(4h+3\alpha)^2}{4}$, $\lambda_2 = -\frac{3\alpha(-32h^3-24h^2\alpha+4h\alpha^2+3\alpha^3)}{2}$, $\lambda_3 = \frac{\alpha^2(-16h^2+9\alpha^2)}{4}$, $\lambda_4 = 9(-8h^2+\alpha^2)^2$,

$\lambda_5 = -\frac{3\alpha(32h^3-24h^2\alpha-4h\alpha^2+3\alpha^3)}{2}$ and $\lambda_6 = \frac{(4h-3\alpha)^2\alpha^2}{4}$. To this end, we have completed the discretization of Eq (4.1) by the multiple varying bounds integral method.

4.1.2. Field 2

We divide the wood boundary into three parts: Faces, vertices, and edges. We found that $\frac{\partial V}{\partial n}$ is discontinuous in these fields, so direct integral cannot be performed and special treatment is required.

1) Analysis about faces of wood.

The wood has a total of six faces. We use the upper face as an example. The other faces follow in a similar fashion. By the Taylor expansion exterior to the upper face, we have

$$V_{i,j,k+1} = V_{i,j,k} + h \cdot V'_{i,j,k} + \frac{1}{2} h^2 \cdot V''_{i,j,k}, \tag{4.8}$$

and

$$V_{i,j,k+2} = V_{i,j,k} + 2h \cdot V'_{i,j,k} + \frac{1}{2}(2h)^2 \cdot V''_{i,j,k}. \tag{4.9}$$

From Eqs (4.8) and (4.9), it follows that

$$V'_{i,j,k} = \frac{4V_{i,j,k+1} - V_{i,j,k+2} - 3V_{i,j,k}}{2h}. \tag{4.10}$$

Similarly, within the interior of the upper face of the wood, there are

$$V'_{i,j,k} = \frac{V_{i,j,k-2} - 4V_{i,j,k-1} + 3V_{i,j,k}}{2h}. \tag{4.11}$$

Since the upper face is horizontal, the $V'_{i,j,k}$ direction is vertical. Thus, $V'_{i,j,k} = \frac{\partial V}{\partial n}$. Consequently, $\varepsilon \frac{\partial V}{\partial n}\Big|_{\partial B_{in}} = \tilde{\varepsilon} \frac{\partial V}{\partial n}\Big|_{\partial B_{out}}$ can be rewritten as

$$\varepsilon V_{i,j,k-2} - 4\varepsilon V_{i,j,k-1} + 3(\varepsilon + \tilde{\varepsilon}) V_{i,j,k} - 4\tilde{\varepsilon} V_{i,j,k+1} + \tilde{\varepsilon} V_{i,j,k+2} = 0. \tag{4.12}$$

Similarly, we can obtain the discrete equations for the other 5 faces of the wood.

2) Analysis about vertices of wood.

The wood has a total of eight vertices. We use the upper front right vertex of the wood as an example. By model (3.1), there is

$$0 = \varepsilon \iint_{\Omega_1} \frac{\partial V}{\partial n} ds + \tilde{\varepsilon} \iint_{\Omega_2} \frac{\partial V}{\partial n} ds = \varepsilon \iint_{\Omega_1} \frac{\partial V}{\partial n} ds + \tilde{\varepsilon} \iint_{\Omega_{21}} \frac{\partial V}{\partial n} ds + \tilde{\varepsilon} \iint_{\Omega_{22}} \frac{\partial V}{\partial n} ds + \tilde{\varepsilon} \iint_{\Omega_{23}} \frac{\partial V}{\partial n} ds. \tag{4.13}$$

This is assuming that Ω represents a spherical surface with its center at the upper front right vertex and a radius of h. Ω_1 and Ω_2 denote the parts of Ω interior and exterior the wood, respectively. There are $\Omega_1 = \frac{1}{8}\Omega$ and $\Omega_2 = \frac{7}{8}\Omega$. Ω_2 can also be divided into three parts based on the vertices, edges, and faces into three parts, that is $\Omega_2 = \Omega_{21} + \Omega_{22} + \Omega_{23}$. Moreover, $\Omega_{21} = \frac{1}{8}\Omega$, $\Omega_{22} = \frac{1}{4}\Omega$, and $\Omega_{23} = \frac{1}{2}\Omega$, as shown in Figure 4.

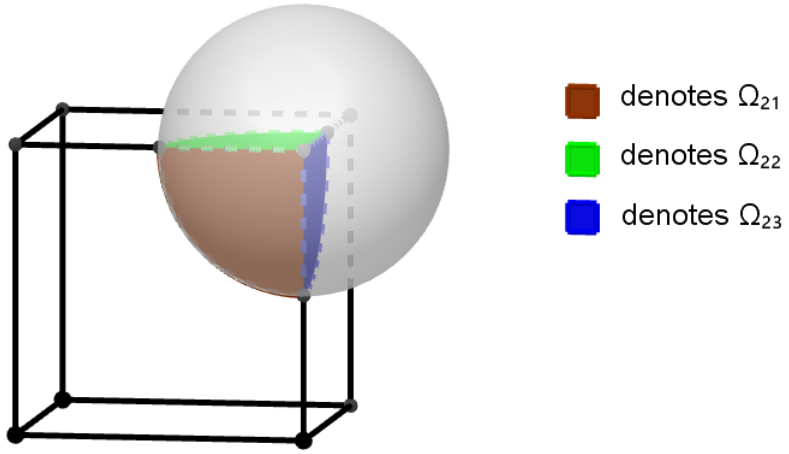

Figure 4. Field division when processing vertices.

From $\frac{\partial V}{\partial n} = \frac{\partial V}{\partial x}\cos\alpha + \frac{\partial V}{\partial y}\cos\beta + \frac{\partial V}{\partial z}\cos\gamma$, we have Eq (4.13), which can be written as

$$\begin{aligned}&\varepsilon\iint_{\Omega_1}(\frac{\partial V}{\partial x}dydz + \frac{\partial V}{\partial y}dxdz + \frac{\partial V}{\partial z}dxdy) + \tilde{\varepsilon}\iint_{\Omega_{21}}(\frac{\partial V}{\partial x}dydz + \frac{\partial V}{\partial y}dxdz + \frac{\partial V}{\partial z}dxdy)\\ &+\tilde{\varepsilon}\iint_{\Omega_{22}}(\frac{\partial V}{\partial x}dydz + \frac{\partial V}{\partial y}dxdz + \frac{\partial V}{\partial z}dxdy) + \tilde{\varepsilon}\iint_{\Omega_{23}}(\frac{\partial V}{\partial x}dydz + \frac{\partial V}{\partial y}dxdz + \frac{\partial V}{\partial z}dxdy) = 0.\end{aligned} \tag{4.14}$$

Next, we discuss each of the items in Eq (4.14).

(i) Consider the interior of the sphere

Take $\iint_{\Omega_1}\frac{\partial V}{\partial x}dydz$ as an example. When calculating $\iint_{\Omega_1}\frac{\partial V}{\partial x}dydz$, we take (x_i, y_j, z_k) as the center and extend two steps in the negative x, y, and z directions, with a step length of $2h$. We define the upper front right vertex as (x_0, y_0, z_0). At this point, 27 points (x_0, y_0, z_0), (x_0, y_0, z_{-1}), (x_0, y_0, z_{-2}), (x_0, y_{-1}, z_0), (x_0, y_{-1}, z_{-1}), (x_0, y_{-1}, z_{-2}), (x_0, y_{-2}, z_0), (x_0, y_{-2}, z_{-1}), (x_0, y_{-2}, z_{-2}), (x_{-1}, y_0, z_0), (x_{-1}, y_0, z_{-1}), (x_{-1}, y_0, z_{-2}), (x_{-1}, y_{-1}, z_0), (x_{-1}, y_{-1}, z_{-1}), (x_{-1}, y_{-1}, z_{-2}), (x_{-1}, y_{-2}, z_0), (x_{-1}, y_{-2}, z_{-1}), (x_{-1}, y_{-2}, z_{-2}), (x_{-2}, y_0, z_0), (x_{-2}, y_0, z_{-1}), (x_{-2}, y_0, z_{-2}), (x_{-2}, y_{-1}, z_0), (x_{-2}, y_{-1}, z_{-1}), (x_{-2}, y_{-1}, z_{-2}), (x_{-2}, y_{-2}, z_0), (x_{-2}, y_{-2}, z_{-1}), (x_{-2}, y_{-2}, z_{-2}) inside the wood are selected for interpolation, as shown in Figure 5.

The interpolation function is

$$\begin{aligned}\frac{\partial V}{\partial x} &= \sum_{i=-2}^{0}\sum_{j=-2}^{0}\sum_{k=-2}^{0}[(\frac{\partial V}{\partial x}\Big|_{i,j,k})\prod_{\substack{m=-2\\m\neq i}}^{0}\frac{x-x_m}{x_i-x_m}\prod_{\substack{s=-2\\s\neq j}}^{0}\frac{y-y_s}{y_j-y_s}\prod_{\substack{t=-2\\t\neq k}}^{0}\frac{z-z_t}{z_k-z_t}]\\ &= \frac{1}{h^6}\sum_{i=-2}^{0}\sum_{j=-2}^{0}\sum_{k=-2}^{0}[(\frac{\partial V}{\partial x}\Big|_{i,j,k})\prod_{\substack{m=-2\\m\neq i}}^{0}\frac{x-x_m}{i-m}\prod_{\substack{s=-2\\s\neq j}}^{0}\frac{y-y_s}{j-s}\prod_{\substack{t=-2\\t\neq k}}^{0}\frac{z-z_t}{k-t}].\end{aligned} \tag{4.15}$$

Since $\frac{\partial V}{\partial x}|_{i,j,k}$ is unknown, it is represented by the difference quotient, and we have

$$\frac{\partial V}{\partial x}\Big|_{i,j,k} = \frac{V_{i,j,k} - V_{i-1,j,k}}{h}. \tag{4.16}$$

In that case,

$$\frac{\partial V}{\partial x} = \frac{1}{h^7}\sum_{i=-2}^{0}\sum_{j=-2}^{0}\sum_{k=-2}^{0}[(V_{i,j,k} - V_{i-1,j,k})\prod_{\substack{m=-2\\m\neq i}}^{0}\frac{x-x_m}{i-m}\prod_{\substack{s=-2\\s\neq j}}^{0}\frac{y-y_s}{j-s}\prod_{\substack{t=-2\\t\neq k}}^{0}\frac{z-z_t}{k-t}], \tag{4.17}$$

then there is

$$\begin{aligned}&\iint_{\Omega_1}\frac{\partial V}{\partial x}dydz\\ &= -\frac{1}{h^7}\sum_{j=-2}^{0}\sum_{k=-2}^{0}[\frac{1}{2}(V_{0,j,k} - V_{-1,j,k})A_1 - (V_{-1,j,k} - V_{-2,j,k})A_2 + \frac{1}{2}(V_{-2,j,k} - V_{-3,j,k})A_3].\end{aligned} \tag{4.18}$$

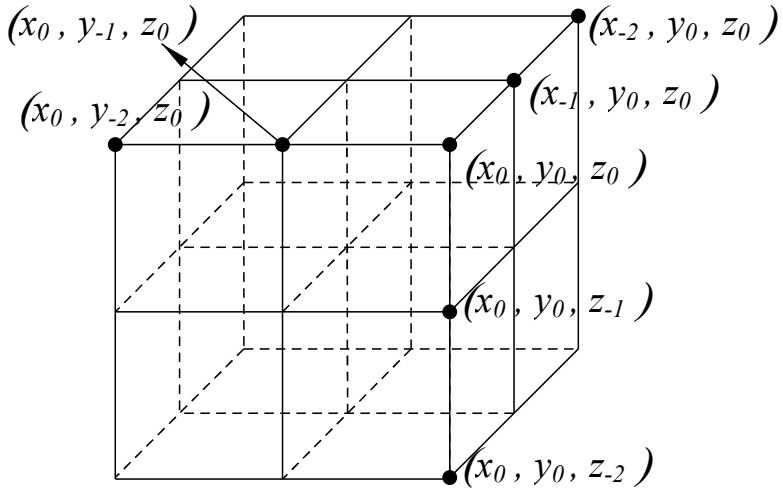

Figure 5. The interpolation points used when handling the vertex and calculating Ω_1.

The integration domain of A_1 can be seen according to the *yoz* plane of Figure 6, so there is

$$A_1 = \int_0^h\int_\pi^{\frac{3\pi}{2}}[(-\sqrt{h^2-\rho^2}+2h)(-\sqrt{h^2-\rho^2}+h)\prod_{\substack{s=-2\\s\neq j}}^{0}(\frac{\rho\cos\theta - sh}{j-s})\prod_{\substack{t=-2\\t\neq k}}^{0}(\frac{\rho\sin\theta - th}{k-t})]\rho d\rho d\theta. \tag{4.19}$$

The same reasoning leads to

$$A_2 = \int_0^h\int_\pi^{\frac{3\pi}{2}}[(-\sqrt{h^2-\rho^2})(-\sqrt{h^2-\rho^2}+2h)\prod_{\substack{s=-2\\s\neq j}}^{0}(\frac{\rho\cos\theta - sh}{j-s})\prod_{\substack{t=-2\\t\neq k}}^{0}(\frac{\rho\sin\theta - th}{k-t})]\rho d\rho d\theta, \tag{4.20}$$

and

$$A_3 = \int_0^h\int_\pi^{\frac{3\pi}{2}}[(-\sqrt{h^2-\rho^2})(-\sqrt{h^2-\rho^2}+h)\prod_{\substack{s=-2\\s\neq j}}^{0}(\frac{\rho\cos\theta - sh}{j-s})\prod_{\substack{t=-2\\t\neq k}}^{0}(\frac{\rho\sin\theta - th}{k-t})]\rho d\rho d\theta. \tag{4.21}$$

Further simplification and organization gives

$$\iint_{\Omega_1} \frac{\partial V}{\partial x}\, dydz = -\sum_{i=-2}^{0}\sum_{j=-2}^{0}\sum_{k=-2}^{0} \frac{1}{h^7}\left(V_{i,j,k} - V_{i-1,j,k}\right) B_1, \tag{4.22}$$

where,

$$B_1 = \int_0^h \int_\pi^{\frac{3\pi}{2}} [\prod_{\substack{m=-2\\ m\neq i}}^{0} (\frac{-\sqrt{h^2-\rho^2} - mh}{i-m}) \prod_{\substack{s=-2\\ s\neq j}}^{0} (\frac{\rho\cos\theta - sh}{j-s}) \prod_{\substack{t=-2\\ t\neq k}}^{0} (\frac{\rho\sin\theta - th}{k-t})]\rho d\rho d\theta. \tag{4.23}$$

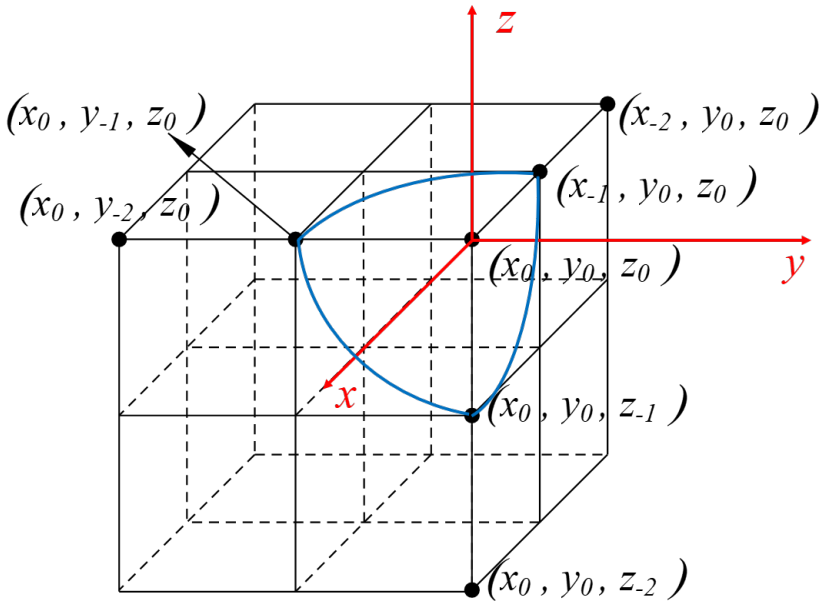

Figure 6. Ω_1 in the coordinate system.

Similarly, when calculating $\iint\limits_{\Omega_1} \frac{\partial V}{\partial y}\, dxdz$ and $\iint\limits_{\Omega_1} \frac{\partial V}{\partial z}\, dxdy$, it is also necessary to construct an interpolation function. The interpolation nodes used for this purpose are illustrated in Figure 5. Thus, there are

$$\iint_{\Omega_1} \frac{\partial V}{\partial y} dxdz = -\sum_{i=-2}^{0}\sum_{j=-2}^{0}\sum_{k=-2}^{0} \frac{1}{h^7}\left(V_{i,j,k} - V_{i,j-1,k}\right) B_2, \tag{4.24}$$

and

$$\iint_{\Omega_1} \frac{\partial V}{\partial z} dxdy = -\sum_{i=-2}^{0}\sum_{j=-2}^{0}\sum_{k=-2}^{0} \frac{1}{h^7}\left(V_{i,j,k} - V_{i,j,k-1}\right) B_3, \tag{4.25}$$

among them,

$$B_2 = \int_0^h \int_\pi^{\frac{3\pi}{2}} [\prod_{\substack{m=-2\\ m\neq i}}^{0} (\frac{\rho\sin\theta - mh}{i-m}) \prod_{\substack{s=-2\\ s\neq j}}^{0} (\frac{-\sqrt{h^2-\rho^2} - sh}{j-s}) \prod_{\substack{t=-2\\ t\neq k}}^{0} (\frac{\rho\cos\theta - th}{k-t})]\rho d\rho d\theta, \tag{4.26}$$

and

$$B_3 = \int_0^h \int_\pi^{\frac{3\pi}{2}} [\prod_{\substack{m=-2 \\ m\neq i}}^{0} (\frac{\rho\cos\theta - mh}{i-m}) \prod_{\substack{s=-2 \\ s\neq j}}^{0} (\frac{\rho\sin\theta - sh}{j-s}) \prod_{\substack{t=-2 \\ t\neq k}}^{0} (\frac{-\sqrt{h^2-\rho^2} - th}{k-t})]\rho d\rho d\theta. \tag{4.27}$$

Therefore,

$$\begin{aligned} &\iint_{\Omega_1} (\frac{\partial V}{\partial x} dydz + \frac{\partial V}{\partial y} dxdz + \frac{\partial V}{\partial z} dxdy) \\ &= -\frac{1}{h^7} \sum_{i=-2}^{0} \sum_{j=-2}^{0} \sum_{k=-2}^{0} \left[\left(V_{i,j,k} - V_{i-1,j,k}\right) B_1 + \left(V_{i,j,k} - V_{i,j-1,k}\right) B_2 + \left(V_{i,j,k} - V_{i,j,k-1}\right) B_3 \right]. \end{aligned} \tag{4.28}$$

We have completed the discretization at Ω_1.

(ii) Consider the exterior of the sphere

We use the method for calculating Ω_1 to compute the integral on Ω_{2i} $(i = 1, 2, 3)$. First, consider field Ω_{21}. We need to interpolate around it by selecting 27 points (x_0, y_0, z_0), (x_0, y_0, z_1), (x_0, y_0, z_2), (x_0, y_{-1}, z_0), (x_0, y_{-1}, z_1), (x_0, y_{-1}, z_2), (x_0, y_{-2}, z_0), (x_0, y_{-2}, z_1), (x_0, y_{-2}, z_2), (x_{-1}, y_0, z_0), (x_{-1}, y_0, z_1), (x_{-1}, y_0, z_2), (x_{-1}, y_{-1}, z_0), (x_{-1}, y_{-1}, z_1), (x_{-1}, y_{-1}, z_2), (x_{-1}, y_{-2}, z_0), (x_{-1}, y_{-2}, z_1), (x_{-1}, y_{-2}, z_2), (x_{-2}, y_0, z_0), (x_{-2}, y_0, z_1), (x_{-2}, y_0, z_2), (x_{-2}, y_{-1}, z_0), (x_{-2}, y_{-1}, z_1), (x_{-2}, y_{-1}, z_2), (x_{-2}, y_{-2}, z_0), (x_{-2}, y_{-2}, z_1), (x_{-2}, y_{-2}, z_2) on the exterior of the wood, as shown in Figure 7.

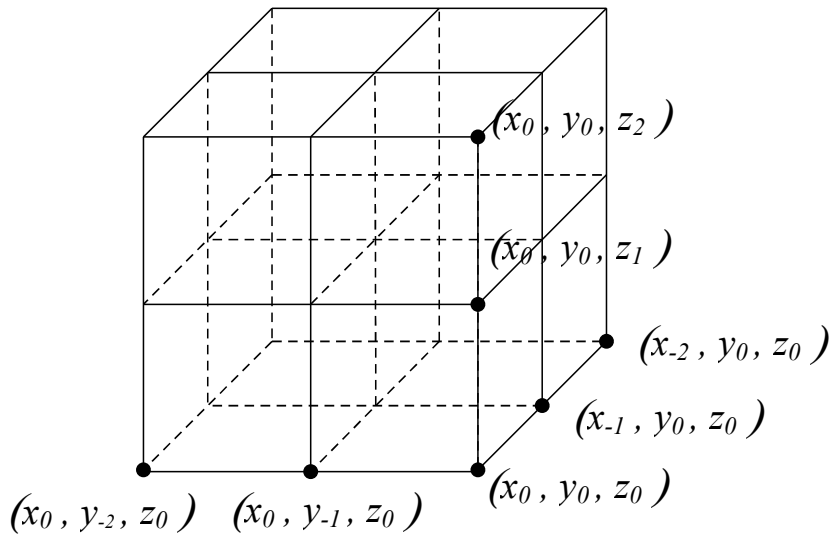

Figure 7. The interpolation points used when handling the vertex and calculating Ω_{21}.

At this point, the interpolating polynomial constructed are

$$\begin{aligned}\frac{\partial V}{\partial x} &= \sum_{i=-2}^{0}\sum_{j=-2}^{0}\sum_{k=0}^{2}[(\frac{\partial V}{\partial x}\Big|_{i,j,k})\prod_{\substack{m=-2\\m\neq i}}^{0}\frac{x-x_m}{x_i-x_m}\prod_{\substack{s=-2\\s\neq j}}^{0}\frac{y-y_s}{y_j-y_s}\prod_{\substack{t=0\\t\neq k}}^{2}\frac{z-z_t}{z_k-z_t}]\\ &= \frac{1}{h^6}\sum_{i=-2}^{0}\sum_{j=-2}^{0}\sum_{k=0}^{2}[(\frac{\partial V}{\partial x}\Big|_{i,j,k})\prod_{\substack{m=-2\\m\neq i}}^{0}\frac{x-x_m}{i-m}\prod_{\substack{s=-2\\s\neq j}}^{0}\frac{y-y_s}{j-s}\prod_{\substack{t=0\\t\neq k}}^{2}\frac{z-z_t}{k-t}],\end{aligned} \tag{4.29}$$

$$\begin{aligned}\frac{\partial V}{\partial y} &= \sum_{i=-2}^{0}\sum_{j=-2}^{0}\sum_{k=0}^{2}[(\frac{\partial V}{\partial y}\Big|_{i,j,k})\prod_{\substack{m=-2\\m\neq i}}^{0}\frac{x-x_m}{x_i-x_m}\prod_{\substack{s=-2\\s\neq j}}^{0}\frac{y-y_s}{y_j-y_s}\prod_{\substack{t=0\\t\neq k}}^{2}\frac{z-z_t}{z_k-z_t}]\\ &= \frac{1}{h^6}\sum_{i=-2}^{0}\sum_{j=-2}^{0}\sum_{k=0}^{2}[(\frac{\partial V}{\partial y}\Big|_{i,j,k})\prod_{\substack{m=-2\\m\neq i}}^{0}\frac{x-x_m}{i-m}\prod_{\substack{s=-2\\s\neq j}}^{0}\frac{y-y_s}{j-s}\prod_{\substack{t=0\\t\neq k}}^{2}\frac{z-z_t}{k-t}],\end{aligned} \tag{4.30}$$

and

$$\begin{aligned}\frac{\partial V}{\partial z} &= \sum_{i=-2}^{0}\sum_{j=-2}^{0}\sum_{k=0}^{2}[(\frac{\partial V}{\partial z}\Big|_{i,j,k})\prod_{\substack{m=-2\\m\neq i}}^{0}\frac{x-x_m}{x_i-x_m}\prod_{\substack{s=-2\\s\neq j}}^{0}\frac{y-y_s}{y_j-y_s}\prod_{\substack{t=0\\t\neq k}}^{2}\frac{z-z_t}{z_k-z_t}]\\ &= \frac{1}{h^6}\sum_{i=-2}^{0}\sum_{j=-2}^{0}\sum_{k=0}^{2}[(\frac{\partial V}{\partial z}\Big|_{i,j,k})\prod_{\substack{m=-2\\m\neq i}}^{0}\frac{x-x_m}{i-m}\prod_{\substack{s=-2\\s\neq j}}^{0}\frac{y-y_s}{j-s}\prod_{\substack{t=0\\t\neq k}}^{2}\frac{z-z_t}{k-t}].\end{aligned} \tag{4.31}$$

Thus, we can get

$$\begin{aligned}&\iint_{\Omega_{21}}(\frac{\partial V}{\partial x}dydz+\frac{\partial V}{\partial y}dxdz+\frac{\partial V}{\partial z}dxdy)\\ &=-\frac{1}{h^7}\sum_{i=-2}^{0}\sum_{j=-2}^{0}\sum_{k=0}^{2}\Big[\Big(V_{i,j,k}-V_{i-1,j,k}\Big)B_4+\Big(V_{i,j,k}-V_{i,j-1,k}\Big)B_5-\Big(V_{i,j,k+1}-V_{i,j,k}\Big)B_6\Big],\end{aligned} \tag{4.32}$$

where,

$$B_4=\int_0^h\int_{\frac{\pi}{2}}^{\pi}[\prod_{\substack{m=-2\\m\neq i}}^{0}(\frac{-\sqrt{h^2-\rho^2}-mh}{i-m})\prod_{\substack{s=-2\\s\neq j}}^{0}(\frac{\rho\cos\theta-sh}{j-s})\prod_{\substack{t=0\\t\neq k}}^{2}(\frac{\rho\sin\theta-th}{k-t})]\rho d\rho d\theta, \tag{4.33}$$

$$B_5=\int_0^h\int_{\frac{3\pi}{2}}^{2\pi}[\prod_{\substack{m=-2\\m\neq i}}^{0}(\frac{\rho\sin\theta-mh}{i-m})\prod_{\substack{s=-2\\s\neq j}}^{0}(\frac{-\sqrt{h^2-\rho^2}-sh}{j-s})\prod_{\substack{t=0\\t\neq k}}^{2}(\frac{\rho\cos\theta-th}{k-t})]\rho d\rho d\theta, \tag{4.34}$$

and

$$B_6=\int_0^h\int_{\pi}^{\frac{3\pi}{2}}[\prod_{\substack{m=-2\\m\neq i}}^{0}(\frac{\rho\cos\theta-mh}{i-m})\prod_{\substack{s=-2\\s\neq j}}^{0}(\frac{\rho\sin\theta-sh}{j-s})\prod_{\substack{t=0\\t\neq k}}^{2}(\frac{\sqrt{h^2-\rho^2}-th}{k-t})]\rho d\rho d\theta. \tag{4.35}$$

Next, consider field Ω_{22}, as shown in Figure 8.

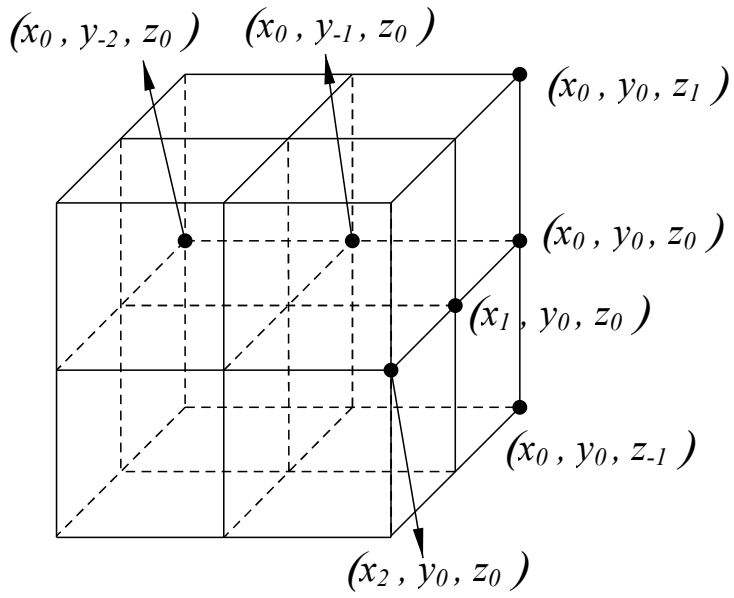

Figure 8. The interpolation points used when handling the vertex and calculating Ω_{22}.

Thus, we obtain

$$\begin{aligned}&\iint_{\Omega_{22}}(\frac{\partial V}{\partial x}dydz+\frac{\partial V}{\partial y}dxdz+\frac{\partial V}{\partial z}dxdy)\\&=\frac{1}{h^7}\sum_{i=0}^{2}\sum_{j=-2}^{0}\sum_{k=-1}^{1}[\left(V_{i+1,j,k}-V_{i,j,k}\right)B_7-\left(V_{i,j,k}-V_{i,j-1,k}\right)B_8+\left(V_{i,j,k+1}-V_{i,j,k}\right)(B_9-B_{10})],\end{aligned}\tag{4.36}$$

where,

$$B_7=\int_0^h\int_{\frac{\pi}{2}}^{\frac{3\pi}{2}}[\prod_{\substack{m=0\\m\neq i}}^{2}(\frac{\sqrt{h^2-\rho^2}-mh}{i-m})\prod_{\substack{s=-2\\s\neq j}}^{0}(\frac{\rho\cos\theta-sh}{j-s})\prod_{\substack{t=-1\\t\neq k}}^{1}(\frac{\rho\sin\theta-th}{k-t})]\rho d\rho d\theta,\tag{4.37}$$

$$B_8=\int_0^h\int_0^{\pi}[\prod_{\substack{m=0\\m\neq i}}^{2}(\frac{\rho\sin\theta-mh}{i-m})\prod_{\substack{s=-2\\s\neq j}}^{0}(\frac{-\sqrt{h^2-\rho^2}-sh}{j-s})\prod_{\substack{t=-1\\t\neq k}}^{1}(\frac{\rho\cos\theta-th}{k-t})]\rho d\rho d\theta,\tag{4.38}$$

$$B_9=\int_0^h\int_{\frac{3\pi}{2}}^{2\pi}[\prod_{\substack{m=0\\m\neq i}}^{2}(\frac{\rho\cos\theta-mh}{i-m})\prod_{\substack{s=-2\\s\neq j}}^{0}(\frac{\rho\sin\theta-sh}{j-s})\prod_{\substack{t=-1\\t\neq k}}^{1}(\frac{\sqrt{h^2-\rho^2}-th}{k-t})]\rho d\rho d\theta,\tag{4.39}$$

and

$$B_{10}=\int_0^h\int_{\frac{3\pi}{2}}^{2\pi}[\prod_{\substack{m=0\\m\neq i}}^{2}(\frac{\rho\cos\theta-mh}{i-m})\prod_{\substack{s=-2\\s\neq j}}^{0}(\frac{\rho\sin\theta-sh}{j-s})\prod_{\substack{t=-1\\t\neq k}}^{1}(\frac{-\sqrt{h^2-\rho^2}-th}{k-t})]\rho d\rho d\theta.\tag{4.40}$$

Finally, consider region Ω_{23}, as shown in Figure 9.

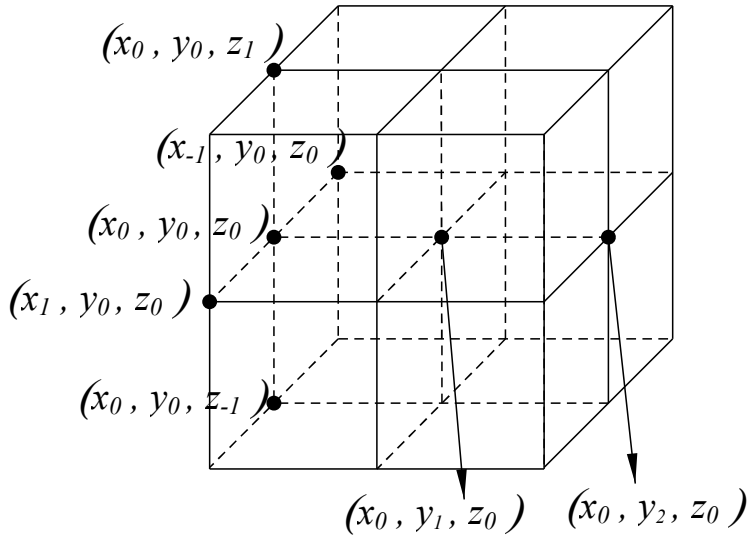

Figure 9. The interpolation points used when handling the vertex and calculating Ω_{23}.

We can get

$$\begin{aligned}&\iint_{\Omega_{23}}(\frac{\partial V}{\partial x}dydz+\frac{\partial V}{\partial y}dxdz+\frac{\partial V}{\partial z}dxdy)\\&=\frac{1}{h^7}\sum_{i=-1}^{1}\sum_{j=0}^{2}\sum_{k=-1}^{1}[\left(V_{i+1,j,k}-V_{i,j,k}\right)(B_{11}-B_{12})+\left(V_{i,j+1,k}-V_{i,j,k}\right)B_{13}+\left(V_{i,j,k+1}-V_{i,j,k}\right)(B_{14}-B_{15})],\end{aligned}\tag{4.41}$$

among it,

$$B_{11}=\int_0^h\int_{-\frac{\pi}{2}}^{\frac{\pi}{2}}[\prod_{\substack{m=-1\\m\neq i}}^{1}(\frac{\sqrt{h^2-\rho^2}-mh}{i-m})\prod_{\substack{s=0\\s\neq j}}^{2}(\frac{\rho\cos\theta-sh}{j-s})\prod_{\substack{t=-1\\t\neq k}}^{1}(\frac{\rho\sin\theta-th}{k-t})]\rho d\rho d\theta,\tag{4.42}$$

$$B_{12}=\int_0^h\int_{-\frac{\pi}{2}}^{\frac{\pi}{2}}[\prod_{\substack{m=-1\\m\neq i}}^{1}(\frac{-\sqrt{h^2-\rho^2}-mh}{i-m})\prod_{\substack{s=0\\s\neq j}}^{2}(\frac{\rho\cos\theta-sh}{j-s})\prod_{\substack{t=-1\\t\neq k}}^{1}(\frac{\rho\sin\theta-th}{k-t})]\rho d\rho d\theta,\tag{4.43}$$

$$B_{13}=\int_0^h\int_0^{2\pi}[\prod_{\substack{m=-1\\m\neq i}}^{1}(\frac{\rho\sin\theta-mh}{i-m})\prod_{\substack{s=0\\s\neq j}}^{2}(\frac{\sqrt{h^2-\rho^2}-sh}{j-s})\prod_{\substack{t=-1\\t\neq k}}^{1}(\frac{\rho\cos\theta-th}{k-t})]\rho d\rho d\theta,\tag{4.44}$$

$$B_{14}=\int_0^h\int_0^{\pi}[\prod_{\substack{m=-1\\m\neq i}}^{1}(\frac{\rho\cos\theta-mh}{i-m})\prod_{\substack{s=0\\s\neq j}}^{2}(\frac{\rho\sin\theta-sh}{j-s})\prod_{\substack{t=-1\\t\neq k}}^{1}(\frac{\sqrt{h^2-\rho^2}-th}{k-t})]\rho d\rho d\theta,\tag{4.45}$$

and

$$B_{15} = \int_0^h \int_0^{\pi} [\prod_{\substack{m=-1 \\ m\neq i}}^{1} (\frac{\rho\cos\theta - mh}{i-m}) \prod_{\substack{s=0 \\ s\neq j}}^{2} (\frac{\rho\sin\theta - sh}{j-s}) \prod_{\substack{t=-1 \\ t\neq k}}^{1} (\frac{-\sqrt{h^2-\rho^2} - th}{k-t})]\rho d\rho d\theta. \tag{4.46}$$

Consequently, Eqs (4.28), (4.32), (4.36), and (4.41) constitute the discrete scheme of the upper front right vertex Eq (4.13). After rearrangement, we have

$$\begin{aligned}
&-\varepsilon \sum_{i=-2}^{0}\sum_{j=-2}^{0}\sum_{k=-2}^{0}[\left(V_{i,j,k}-V_{i-1,j,k}\right)B_1+\left(V_{i,j,k}-V_{i,j-1,k}\right)B_2+\left(V_{i,j,k}-V_{i,j,k-1}\right)B_3]\\
&-\tilde{\varepsilon} \sum_{i=-2}^{0}\sum_{j=-2}^{0}\sum_{k=0}^{2}[\left(V_{i,j,k}-V_{i-1,j,k}\right)B_4+\left(V_{i,j,k}-V_{i,j-1,k}\right)B_5-\left(V_{i,j,k+1}-V_{i,j,k}\right)B_6]\\
&+\tilde{\varepsilon} \sum_{i=0}^{2}\sum_{j=-2}^{0}\sum_{k=-1}^{1}[\left(V_{i+1,j,k}-V_{i,j,k}\right)B_7-\left(V_{i,j,k}-V_{i,j-1,k}\right)B_8+\left(V_{i,j,k+1}-V_{i,j,k}\right)(B_9-B_{10})]\\
&+\tilde{\varepsilon} \sum_{i=-1}^{1}\sum_{j=0}^{2}\sum_{k=-1}^{1}[\left(V_{i+1,j,k}-V_{i,j,k}\right)(B_{11}-B_{12})+\left(V_{i,j+1,k}-V_{i,j,k}\right)B_{13}+\left(V_{i,j,k+1}-V_{i,j,k}\right)(B_{14}-B_{15})]=0.
\end{aligned} \tag{4.47}$$

Similarly, discrete schemes for the other 7 vertices can be obtained.

3) Analysis about edges of wood.

The wood has twelve edges. We use the upper right edge of the wood as an example. By model (3.1), there is

$$0 = \varepsilon \iint_{\Omega_1} \frac{\partial V}{\partial n} ds + \tilde{\varepsilon} \iint_{\Omega_2} \frac{\partial V}{\partial n} ds = \varepsilon \iint_{\Omega_1} \frac{\partial V}{\partial n} ds + \tilde{\varepsilon} \iint_{\Omega_{21}} \frac{\partial V}{\partial n} ds + \tilde{\varepsilon} \iint_{\Omega_{22}} \frac{\partial V}{\partial n} ds, \tag{4.48}$$

where Ω denotes a cylindrical surface with the upper right edge as the axis and h as the radius. Ω_1 and Ω_2 denote the parts of Ω in the interior and exterior of the wood, respectively. There are $\Omega_1 = \frac{1}{4}\Omega$ and $\Omega_2 = \frac{3}{4}\Omega$. Ω_2 is also divided into two parts according to the edges and faces, that is $\Omega_2 = \Omega_{21} + \Omega_{22}$, where $\Omega_{21} = \frac{1}{4}\Omega$ and $\Omega_{22} = \frac{1}{2}\Omega$, as illustrated in Figure 10.

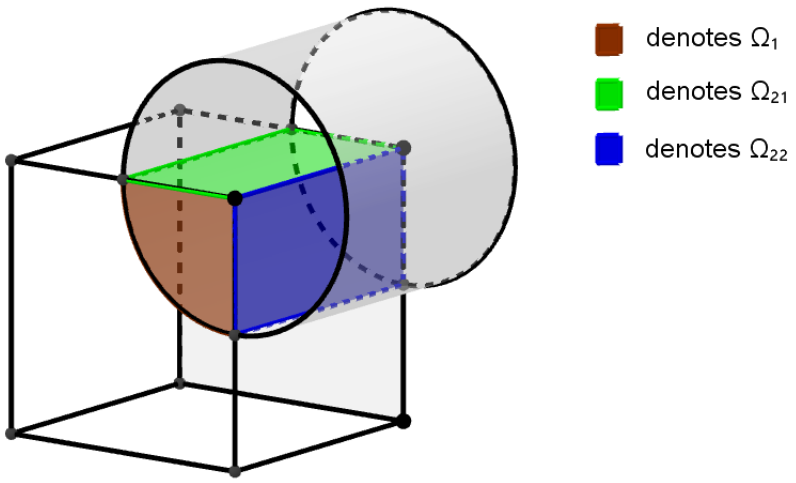

Figure 10. Field division when processing edges.

First, consider region Ω_1. We need to interpolate around it by selecting 27 points (x_0, y_0, z_0), (x_0, y_0, z_{-2}), (x_0, y_0, z_{-1}), (x_0, y_{-1}, z_0), (x_0, y_{-1}, z_{-1}), (x_0, y_{-1}, z_{-2}), (x_0, y_{-2}, z_0), (x_0, y_{-2}, z_{-1}), (x_0, y_{-2}, z_{-2}), (x_1, y_0, z_0), (x_1, y_0, z_{-1}), (x_1, y_0, z_{-2}), (x_1, y_{-1}, z_0), (x_1, y_{-1}, z_{-1}), (x_1, y_{-1}, z_{-2}), (x_1, y_{-2}, z_0), (x_1, y_{-2}, z_{-1}), (x_1, y_{-2}, z_{-2}), (x_2, y_0, z_0), (x_2, y_0, z_{-1}), (x_2, y_0, z_{-2}), (x_2, y_{-1}, z_0), (x_2, y_{-1}, z_{-1}), (x_2, y_{-1}, z_{-2}), (x_2, y_{-2}, z_0), (x_2, y_{-2}, z_{-1}), (x_2, y_{-2}, z_{-2}) on the interior of the wood as shown in Figure 11.

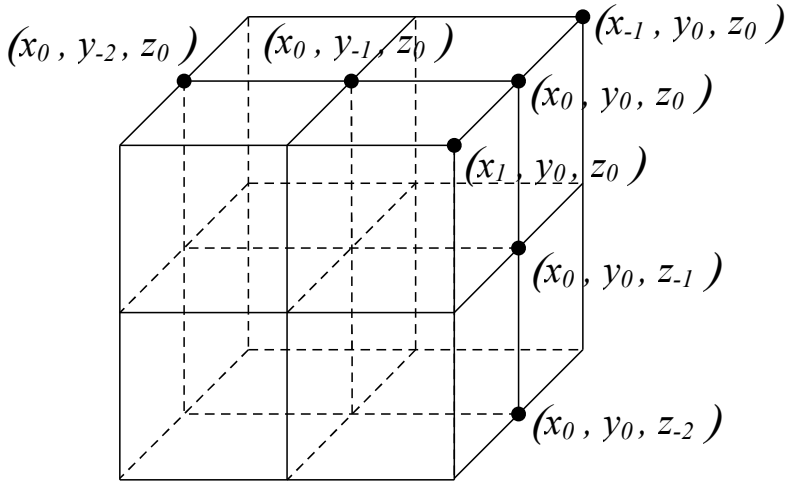

Figure 11. The interpolation points used when handling the edge and calculating Ω_1.

The interpolating polynomial constructed are

$$\begin{aligned}\frac{\partial V}{\partial x} &= \sum_{i=-1}^{1}\sum_{j=-2}^{0}\sum_{k=-2}^{0}[(\frac{\partial V}{\partial x}\Big|_{i,j,k})\prod_{\substack{m=-1\\m\neq i}}^{1}\frac{x-x_m}{x_i-x_m}\prod_{\substack{s=-2\\s\neq j}}^{0}\frac{y-y_s}{y_j-y_s}\prod_{\substack{t=-2\\t\neq k}}^{0}\frac{z-z_t}{z_k-z_t}]\\ &= \frac{1}{h^6}\sum_{i=-1}^{1}\sum_{j=-2}^{0}\sum_{k=-2}^{0}[(\frac{\partial V}{\partial x}\Big|_{i,j,k})\prod_{\substack{m=-1\\m\neq i}}^{1}\frac{x-x_m}{i-m}\prod_{\substack{s=-2\\s\neq j}}^{0}\frac{y-y_s}{j-s}\prod_{\substack{t=-2\\t\neq k}}^{0}\frac{z-z_t}{k-t}],\end{aligned} \tag{4.49}$$

$$\begin{aligned}\frac{\partial V}{\partial y} &= \sum_{i=-1}^{1}\sum_{j=-2}^{0}\sum_{k=-2}^{0}[(\frac{\partial V}{\partial y}\Big|_{i,j,k})\prod_{\substack{m=-1\\m\neq i}}^{1}\frac{x-x_m}{x_i-x_m}\prod_{\substack{s=-2\\s\neq j}}^{0}\frac{y-y_s}{y_j-y_s}\prod_{\substack{t=-2\\t\neq k}}^{0}\frac{z-z_t}{z_k-z_t}]\\ &= \frac{1}{h^6}\sum_{i=-1}^{1}\sum_{j=-2}^{0}\sum_{k=-2}^{0}[(\frac{\partial V}{\partial y}\Big|_{i,j,k})\prod_{\substack{m=-1\\m\neq i}}^{1}\frac{x-x_m}{i-m}\prod_{\substack{s=-2\\s\neq j}}^{0}\frac{y-y_s}{j-s}\prod_{\substack{t=-2\\t\neq k}}^{0}\frac{z-z_t}{k-t}],\end{aligned} \tag{4.50}$$

and

$$\begin{aligned}\frac{\partial V}{\partial z} &= \sum_{i=-1}^{1}\sum_{j=-2}^{0}\sum_{k=-2}^{0}[(\frac{\partial V}{\partial z}\Big|_{i,j,k})\prod_{\substack{m=-1\\m\neq i}}^{1}\frac{x-x_m}{x_i-x_m}\prod_{\substack{s=-2\\s\neq j}}^{0}\frac{y-y_s}{y_j-y_s}\prod_{\substack{t=-2\\t\neq k}}^{0}\frac{z-z_t}{z_k-z_t}]\\ &= \frac{1}{h^6}\sum_{i=-1}^{1}\sum_{j=-2}^{0}\sum_{k=-2}^{0}[(\frac{\partial V}{\partial z}\Big|_{i,j,k})\prod_{\substack{m=-1\\m\neq i}}^{1}\frac{x-x_m}{i-m}\prod_{\substack{s=-2\\s\neq j}}^{0}\frac{y-y_s}{j-s}\prod_{\substack{t=-2\\t\neq k}}^{0}\frac{z-z_t}{k-t}].\end{aligned} \tag{4.51}$$

Therefore,

$$\begin{aligned}&\iint_{\Omega_1}\left(\frac{\partial V}{\partial x}dydz+\frac{\partial V}{\partial y}dxdz+\frac{\partial V}{\partial z}dxdy\right)\\&=\frac{1}{h^7}\sum_{i=-1}^{1}\sum_{j=-2}^{0}\sum_{k=-2}^{0}\left[\left(V_{i+1,j,k}-V_{i,j,k}\right)(C_1-C_2)-\left(V_{i,j,k}-V_{i,j-1,k}\right)C_3-\left(V_{i,j,k}-V_{i,j,k-1}\right)C_4\right],\end{aligned}\tag{4.52}$$

where,

$$C_1=\int_0^h\int_\pi^{\frac{3\pi}{2}}\Big[\prod_{\substack{m=-1\\m\neq i}}^{1}\Big(\frac{\sqrt{h^2-\rho^2}-mh}{i-m}\Big)\prod_{\substack{s=-2\\s\neq j}}^{0}\Big(\frac{\rho\cos\theta-sh}{j-s}\Big)\prod_{\substack{t=-2\\t\neq k}}^{0}\Big(\frac{\rho\sin\theta-th}{k-t}\Big)\Big]\rho d\rho d\theta,\tag{4.53}$$

$$C_2=\int_0^h\int_\pi^{\frac{3\pi}{2}}\Big[\prod_{\substack{m=-1\\m\neq i}}^{1}\Big(\frac{-\sqrt{h^2-\rho^2}-mh}{i-m}\Big)\prod_{\substack{s=-2\\s\neq j}}^{0}\Big(\frac{\rho\cos\theta-sh}{j-s}\Big)\prod_{\substack{t=-2\\t\neq k}}^{0}\Big(\frac{\rho\sin\theta-th}{k-t}\Big)\Big]\rho d\rho d\theta,\tag{4.54}$$

$$C_3=\int_0^h\int_{\frac{\pi}{2}}^{\frac{3\pi}{2}}\Big[\prod_{\substack{m=-1\\m\neq i}}^{1}\Big(\frac{\rho\sin\theta-mh}{i-m}\Big)\prod_{\substack{s=-2\\s\neq j}}^{0}\Big(\frac{-\sqrt{h^2-\rho^2}-sh}{j-s}\Big)\prod_{\substack{t=-2\\t\neq k}}^{0}\Big(\frac{\rho\cos\theta-th}{k-t}\Big)\Big]\rho d\rho d\theta,\tag{4.55}$$

and

$$C_4=\int_0^h\int_\pi^{2\pi}\Big[\prod_{\substack{m=-1\\m\neq i}}^{1}\Big(\frac{\rho\cos\theta-mh}{i-m}\Big)\prod_{\substack{s=-2\\s\neq j}}^{0}\Big(\frac{\rho\sin\theta-sh}{j-s}\Big)\prod_{\substack{t=-2\\t\neq k}}^{0}\Big(\frac{-\sqrt{h^2-\rho^2}-th}{k-t}\Big)\Big]\rho d\rho d\theta.\tag{4.56}$$

Second, we consider $\iint_{\Omega_{21}}\frac{\partial V}{\partial n}ds$. The interpolation nodes of field Ω_{21} are shown in Figure 12.

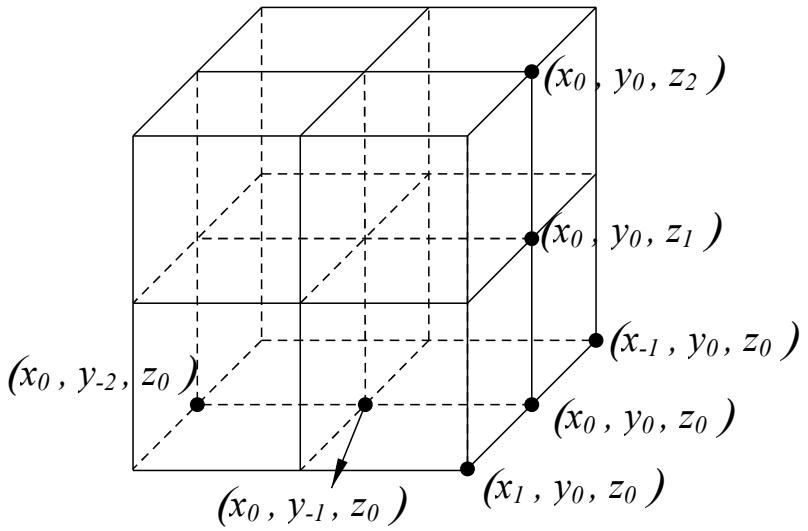

Figure 12. The interpolation points used when handling the edge and calculating Ω_{21}.

Equally,

$$\begin{aligned}&\iint_{\Omega_{21}}\left(\frac{\partial V}{\partial x}dydz+\frac{\partial V}{\partial y}dxdz+\frac{\partial V}{\partial z}dxdy\right)\\&=\frac{1}{h^7}\sum_{i=-1}^{1}\sum_{j=-2}^{0}\sum_{k=0}^{2}\left[\left(V_{i+1,j,k}-V_{i,j,k}\right)(C_5-C_6)-\left(V_{i,j,k}-V_{i,j-1,k}\right)C_7+\left(V_{i,j,k+1}-V_{i,j,k}\right)C_8\right],\end{aligned}\tag{4.57}$$

among it

$$C_5=\int_0^h\int_{\frac{\pi}{2}}^{\pi}[\prod_{\substack{m=-1\\m\neq i}}^{1}(\frac{\sqrt{h^2-\rho^2}-mh}{i-m})\prod_{\substack{s=-2\\s\neq j}}^{0}(\frac{\rho\cos\theta-sh}{j-s})\prod_{\substack{t=0\\t\neq k}}^{2}(\frac{\rho\sin\theta-th}{k-t})]\rho d\rho d\theta,\tag{4.58}$$

$$C_6=\int_0^h\int_{\frac{\pi}{2}}^{\pi}[\prod_{\substack{m=-1\\m\neq i}}^{1}(\frac{-\sqrt{h^2-\rho^2}-mh}{i-m})\prod_{\substack{s=-2\\s\neq j}}^{0}(\frac{\rho\cos\theta-sh}{j-s})\prod_{\substack{t=0\\t\neq k}}^{2}(\frac{\rho\sin\theta-th}{k-t})]\rho d\rho d\theta,\tag{4.59}$$

$$C_7=\int_0^h\int_{-\frac{\pi}{2}}^{\frac{\pi}{2}}[\prod_{\substack{m=-1\\m\neq i}}^{1}(\frac{\rho\sin\theta-mh}{i-m})\prod_{\substack{s=-2\\s\neq j}}^{0}(\frac{-\sqrt{h^2-\rho^2}-sh}{j-s})\prod_{\substack{t=0\\t\neq k}}^{2}(\frac{\rho\cos\theta-th}{k-t})]\rho d\rho d\theta,\tag{4.60}$$

and

$$C_8=\int_0^h\int_{\pi}^{2\pi}[\prod_{\substack{m=-1\\m\neq i}}^{1}(\frac{\rho\cos\theta-mh}{i-m})\prod_{\substack{s=-2\\s\neq j}}^{0}(\frac{\rho\sin\theta-sh}{j-s})\prod_{\substack{t=0\\t\neq k}}^{2}(\frac{\sqrt{h^2-\rho^2}-th}{k-t})]\rho d\rho d\theta.\tag{4.61}$$

Finally, we consider $\iint_{\Omega_{22}}\frac{\partial V}{\partial n}ds$. The interpolation nodes of field Ω_{22} are shown in Figure 13.

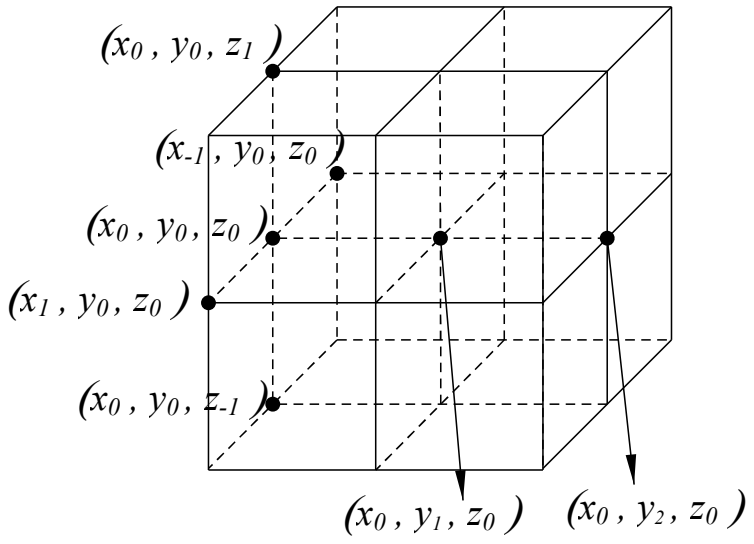

Figure 13. The interpolation points used when handling the edge and calculating Ω_{21}.

With the same way,

$$\begin{aligned}&\iint_{\Omega_{22}}(\frac{\partial V}{\partial x}dydz+\frac{\partial V}{\partial y}dxdz+\frac{\partial V}{\partial z}dxdy)\\&=\frac{1}{h^7}\sum_{i=-1}^{1}\sum_{j=0}^{2}\sum_{k=-1}^{1}[\Big(V_{i+1,j,k}-V_{i,j,k}\Big)(C_9-C_{10})+\Big(V_{i,j+1,k}-V_{i,j,k}\Big)C_{11}+\Big(V_{i,j,k+1}-V_{i,j,k}\Big)(C_{12}-C_{13})],\end{aligned}\tag{4.62}$$

where,

$$C_9=\int_0^h\int_{-\frac{\pi}{2}}^{\frac{\pi}{2}}[\prod_{\substack{m=-1\\m\neq i}}^{1}(\frac{\sqrt{h^2-\rho^2}-mh}{i-m})\prod_{\substack{s=0\\s\neq j}}^{2}(\frac{\rho\cos\theta-sh}{j-s})\prod_{\substack{t=-1\\t\neq k}}^{1}(\frac{\rho\sin\theta-th}{k-t})]\rho d\rho d\theta,\tag{4.63}$$

$$C_{10}=\int_0^h\int_{-\frac{\pi}{2}}^{\frac{\pi}{2}}[\prod_{\substack{m=-1\\m\neq i}}^{1}(\frac{-\sqrt{h^2-\rho^2}-mh}{i-m})\prod_{\substack{s=0\\s\neq j}}^{2}(\frac{\rho\cos\theta-sh}{j-s})\prod_{\substack{t=-1\\t\neq k}}^{1}(\frac{\rho\sin\theta-th}{k-t})]\rho d\rho d\theta,\tag{4.64}$$

$$C_{11}=\int_0^h\int_0^{2\pi}[\prod_{\substack{m=-1\\m\neq i}}^{1}(\frac{\rho\sin\theta-mh}{i-m})\prod_{\substack{s=0\\s\neq j}}^{2}(\frac{\sqrt{h^2-\rho^2}-sh}{j-s})\prod_{\substack{t=-1\\t\neq k}}^{1}(\frac{\rho\cos\theta-th}{k-t})]\rho d\rho d\theta,\tag{4.65}$$

$$C_{12}=\int_0^h\int_0^{\pi}[\prod_{\substack{m=-1\\m\neq i}}^{1}(\frac{\rho\cos\theta-mh}{i-m})\prod_{\substack{s=0\\s\neq j}}^{2}(\frac{\rho\sin\theta-sh}{j-s})\prod_{\substack{t=-1\\t\neq k}}^{1}(\frac{\sqrt{h^2-\rho^2}-th}{k-t})]\rho d\rho d\theta,\tag{4.66}$$

and

$$C_{13}=\int_0^h\int_0^{\pi}[\prod_{\substack{m=-1\\m\neq i}}^{1}(\frac{\rho\cos\theta-mh}{i-m})\prod_{\substack{s=0\\s\neq j}}^{2}(\frac{\rho\sin\theta-sh}{j-s})\prod_{\substack{t=-1\\t\neq k}}^{1}(\frac{-\sqrt{h^2-\rho^2}-th}{k-t})]\rho d\rho d\theta.\tag{4.67}$$

Thus, Eqs (4.52), (4.57), and (4.62) constitute the discrete scheme of the upper right edge Eq (4.48), organized as

$$\begin{aligned}&\varepsilon\sum_{i=1}^{1}\sum_{j=-2}^{0}\sum_{k=-2}^{0}\Big[\Big(V_{i+1,j,k}-V_{i,j,k}\Big)(C_1-C_2)-\Big(V_{i,j,k}-V_{i,j-1,k}\Big)C_3-\Big(V_{i,j,k}-V_{i,j,k-1}\Big)C_4\Big]\\&+\tilde{\varepsilon}\sum_{i=1}^{1}\sum_{j=-2}^{0}\sum_{k=0}^{2}\Big[\Big(V_{i+1,j,k}-V_{i,j,k}\Big)(C_5-C_6)-\Big(V_{i,j,k}-V_{i,j-1,k}\Big)C_7+\Big(V_{i,j,k+1}-V_{i,j,k}\Big)C_8\Big]\\&+\tilde{\varepsilon}\sum_{i=-1}^{1}\sum_{j=0}^{2}\sum_{k=-1}^{1}\Big[\Big(V_{i+1,j,k}-V_{i,j,k}\Big)(C_9-C_{10})+\Big(V_{i,j+1,k}-V_{i,j,k}\Big)C_{11}+\Big(V_{i,j,k+1}-V_{i,j,k}\Big)(C_{12}-C_{13})\Big]=0.\end{aligned}\tag{4.68}$$

Similarly, we can obtain discrete equations for the other 11 edges of the wood.

4.2. Error estimation of discrete schemes

We take the first equation and third equation in system (3.1) as examples for error estimation, and the remaining equations follow a similar approach.

1) Error estimation of the first equation

Since the first equation $\nabla^2 V(x,y,z)=0$ employs the Lagrange interpolation function, the remainder term of the Lagrange interpolation is given by

$$R(x,y,z)=\frac{\partial^9 V(\xi,\eta,\zeta)}{3!3!3!\partial x^3\partial y^3\partial z^3}\prod_{p=i-1}^{i+1}\left(x-x_p\right)\prod_{q=j-1}^{j+1}\left(y-y_q\right)\prod_{r=k-1}^{k+1}\left(z-z_r\right), \tag{4.69}$$

where, $\xi\in(x_{i-1},x_{i+1})$, $\eta\in\left(y_{j-1},y_{j+1}\right)$, $\zeta\in(z_{k-1},z_{k+1})$. If $\left|\frac{\partial^9 V(\xi,\eta,\zeta)}{\partial x^3\partial y^3\partial z^3}\right|\le M$, we have

$$|R(x,y,z)|\le\frac{M}{216}\left|\prod_{p=i-1}^{i+1}\left(x-x_p\right)\prod_{q=j-1}^{j+1}\left(y-y_q\right)\prod_{r=k-1}^{k+1}\left(z-z_r\right)\right|. \tag{4.70}$$

Therefore, the error of the first equation is

$$\left|\int_{z_k-\alpha_z}^{z_k}\int_{z_k}^{z_k+\frac{\alpha_z}{2}}\int_{y_j-\alpha_y}^{y_j}\int_{y_j}^{y_j+\frac{\alpha_y}{2}}\int_{x_i-\alpha_x}^{x_i}\int_{x_i}^{x_i+\frac{\alpha_x}{2}}\left[\int_{z_1}^{z_2}\int_{y_1}^{y_2}\int_{x_1}^{x_2}\left(\frac{\partial^2 R}{\partial x^2}+\frac{\partial^2 R}{\partial y^2}+\frac{\partial^2 R}{\partial z^2}\right)dxdydz\right]dx_2dx_1dy_2dy_1dz_2dz_1\right|. \tag{4.71}$$

Due to the identical structure of the three terms, we perform only the calculation for $\frac{\partial^2 R}{\partial x^2}$, as the other two terms can be computed similarly. First, integrating with respect to x, we have

$$\begin{aligned}
&\int_{x_i-\alpha_x}^{x_i}\int_{x_i}^{x_i+\frac{\alpha_x}{2}}\int_{x_1}^{x_2}\frac{\partial^2 R}{\partial x^2}dxdx_2dx_1\\
&=\int_{x_i-\alpha_x}^{x_i}\int_{x_i}^{x_i+\frac{\alpha_x}{2}}\left(\frac{\partial R}{\partial x_2}-\frac{\partial R}{\partial x_1}\right)dx_2dx_1\\
&=\int_{x_i-\alpha_x}^{x_i}\int_{x_i}^{x_i+\frac{\alpha_x}{2}}\frac{\partial R}{\partial x_2}dx_2dx_1-\int_{x_i-\alpha_x}^{x_i}\int_{x_i}^{x_i+\frac{\alpha_x}{2}}\frac{\partial R}{\partial x_1}dx_2dx_1\\
&=\alpha_x\int_{x_i}^{x_i+\frac{\alpha_x}{2}}\frac{\partial R}{\partial x_2}dx_2-\frac{\alpha_x}{2}\int_{x_i-\alpha_x}^{x_i}\frac{\partial R}{\partial x_1}dx_1\\
&=O(h_x^4).
\end{aligned} \tag{4.72}$$

Next, integrating with respect to y, we have

$$\begin{aligned}
&\int_{y_i-\alpha_y}^{y_j}\int_{y_j}^{y_j+\frac{\alpha_y}{2}}\int_{y_1}^{y_2}(y-y_{j-1})(y-y_j)(y-y_{j+1})dydy_2dy_1\\
&=\int_{y_j-\alpha_y}^{y_j}\int_{y_j}^{y_j+\frac{\alpha_y}{2}}\int_{y_1}^{y_2}(y-y_j-h_y)(y-y_j)(y-y_j+h_y)dydy_2dy_1\\
&=\int_{y_j-\alpha_y}^{y_j}\int_{y_j}^{y_j+\frac{\alpha_y}{2}}\int_{y_1}^{y_2}\left[(y-y_j)^2-h_y^2\right](y-y_j)dydy_2dy_1\\
&=\int_{y_j-\alpha_y}^{y_j}\int_{y_j}^{y_j+\frac{\alpha_y}{2}}\left[\frac{1}{4}(y-y_j)^4-\frac{h_y^2}{2}(y-y_j)^2\right]\Big|_{y_1}^{y_2}dy_2dy_1\\
&=\int_{y_j-\alpha_j}^{y_j}\int_{y_j}^{y_j+\frac{\alpha_y}{2}}\left[\frac{1}{4}(y_2-y_j)^4-\frac{h_y^2}{2}(y_2-y_j)^2-\frac{1}{4}(y_1-y_j)^4+\frac{h_y^2}{2}(y_1-y_j)^2\right]dy_2dy_1.
\end{aligned} \tag{4.73}$$

At this point, integrating with respect to y_2, we have

$$\begin{aligned}
&\int_{y_j-\alpha_y}^{y_j}\int_{y_j}^{y_j+\frac{\alpha_y}{2}}\left[\frac{1}{4}(y_2-y_j)^4-\frac{h_y^2}{2}(y_2-y_j)^2\right]dy_2dy_1\\
&=\alpha_y\int_{y_j}^{y_j+\frac{\alpha_y}{2}}\left[\frac{1}{4}(y_2-y_j)^4-\frac{h_y^2}{2}(y_2-y_j)^2\right]dy_2\\
&=\alpha_y\int_0^{\frac{\alpha_y}{2}}\left(\frac{1}{4}t^4-\frac{h_y^2}{2}t^2\right)dt\\
&=\frac{1}{20\cdot 2^5}\left(\alpha_y\right)^6-\frac{h_y^2}{6\cdot 2^3}\left(\alpha_y\right)^4=O(h_y^6).
\end{aligned}\tag{4.74}$$

Similarly, the integral for y_1 is

$$\int_{y_j-\alpha_y}^{y_j}\int_{\alpha_y}^{y_j+\frac{\alpha_y}{2}}\int_{y_1}^{y_2}(y-y_{j-1})(y-y_j)(y-y_{j+1})dydy_2dy_1=O(h_y^6).\tag{4.75}$$

Likewise, the integral with respect to the z direction is also $O(h_z^6)$. Therefore,

$$\begin{aligned}
&\left|\int_{z_k-\alpha_z}^{z_k}\int_{z_k}^{z_k+\frac{\alpha_z}{2}}\int_{y_j-\alpha_y}^{y_j}\int_{y_j}^{y_j+\frac{\alpha_y}{2}}\int_{x_i-\alpha_x}^{x_i}\int_{x_i}^{x_i+\frac{\alpha_x}{2}}\int_{z_1}^{z_2}\int_{y_1}^{y_2}\int_{x_1}^{x_2}\frac{\partial^2 R}{\partial x^2}dxdydzdx_2dx_1dy_2dy_1dz_2dz_1\right|\\
&=O\left(h_x^4+h_y^6+h_z^6\right).
\end{aligned}\tag{4.76}$$

However, to ensure accuracy, it is also necessary to divide by the integration factor. The integration factor is

$$\int_{z_k-\alpha_z}^{z_k}\int_{z_k}^{z_k+\frac{\alpha_z}{2}}\int_{z_1}^{z_2}dzdz_2dz_1\int_{y_j-\alpha_y}^{y_j}\int_{y_j}^{y_j+\frac{\alpha_y}{2}}\int_{y_1}^{y_2}dydy_2dy_1=O(h_y^3+h_z^3).\tag{4.77}$$

Therefore, the accuracy of Eq (4.76) should be $O(h_x^4+h_y^3+h_z^3)$. Thus, the error of Eq (4.71) is

$$O(h_x^4+h_y^3+h_z^3)+O(h_y^4+h_z^3+h_x^3)+O(h_z^4+h_y^3+h_x^3)=O(h_x^3+h_y^3+h_z^3).$$

Hence, the local truncation error of the discrete scheme is $O(h_x^3+h_y^3+h_z^3)$, and the global error is $O(h_x^2+h_y^2+h_z^2)$.

2) Error estimation of the third equation

By the Taylor expansion, we have

$$V_{i,j,k+1}=V_{i,j,k}+h_zV'_{i,j,k}+\frac{1}{2}h_z^2V''_{i,j,k}+\frac{1}{3!}h_z^3V'''_{i,j,k}+\frac{1}{4!}h_z^4V^{(4)}_{i,j,k},\tag{4.78}$$

$$V_{i,j,k+2}=V_{i,j,k}+2h_zV'_{i,j,k}+\frac{1}{2}(2h_z)^2V''_{i,j,k}+\frac{1}{3!}(2h_z)^3V'''_{i,j,k}+\frac{1}{4!}(2h_z)^4V^{(4)}_{i,j,k},\tag{4.79}$$

$$V_{i,j,k-1}=V_{i,j,k}-h_zV'_{i,j,k}+\frac{1}{2}h_z^2V''_{i,j,k}-\frac{1}{3!}h_z^3V'''_{i,j,k}+\frac{1}{4!}h_z^4V^{(4)}_{i,j,k},\tag{4.80}$$

and

$$V_{i,j,k-2}=V_{i,j,k}-2h_zV'_{i,j,k}+\frac{1}{2}(2h_z)^2V''_{i,j,k}-\frac{1}{3!}(2h_z)^3V'''_{i,j,k}+\frac{1}{4!}(2h_z)^4V^{(4)}_{i,j,k}.\tag{4.81}$$

By $4 \times (4.78) - (4.79)$ and $(4.81) - 4 \times (4.80)$, we eliminate $V''_{i,j,k}$ and obtain

$$V'_{i,j,k} = \frac{4V_{i,j,k+1} - V_{i,j,k+2} - 3V_{i,j,k}}{2h_z} + \frac{1}{3}h_z^2 V'''_{i,j,k} + \frac{1}{4}h_z^3 V^{(4)}_{i,j,k}, \tag{4.82}$$

and

$$V'_{i,j,k} = \frac{V_{i,j,k-2} - 4V_{i,j,k-1} + 3V_{i,j,k}}{2h_z} + \frac{1}{3}h_z^2 V'''_{i,j,k} - \frac{1}{4}h_z^3 V^{(4)}_{i,j,k}. \tag{4.83}$$

Thus,

$$\begin{aligned} &\tilde{\varepsilon}\frac{\partial V}{\partial n}|_{\partial B_{in}} - \varepsilon\frac{\partial V}{\partial n}|_{\partial B_{out}} \\ &= \tilde{\varepsilon}\left(\frac{4V_{i,j,k+1} - V_{i,j,k+2} - 3V_{i,j,k}}{2h_z} + \frac{1}{3}h_z^2 V'''_{i,j,k} + \frac{1}{4}h_z^3 V^{(4)}_{i,j,k}\right) - \varepsilon\left(\frac{V_{i,j,k-2} - 4V_{i,j,k-1} + 3V_{i,j,k}}{2h_z} + \frac{1}{3}h_z^2 V'''_{i,j,k} - \frac{1}{4}h_z^3 V^{(4)}_{i,j,k}\right). \end{aligned} \tag{4.84}$$

In practical situations, $\tilde{\varepsilon} \neq \varepsilon$. Therefore, the error is $O\left(h_z^2\right)$. Similarly, it can be concluded that the error in the x and y directions are $O\left(h_x^2\right)$ and $O\left(h_y^2\right)$. As a result, the third equation error is $O(h_x^2 + h_y^2 + h_z^2)$.

4.3. Numerical analysis

We illustrate the theory in this paper through a numerical example using the multiple varying bounds integral method.

The two electrode plates occupy the domain

$$B_1 = \{(x, y, z) \,|\, -3 \leq x \leq 3, 1 \leq y \leq 6, 0 \leq z \leq 2\},$$

and

$$B_2 = \{(x, y, z) \,|\, -3 \leq x \leq 3, -6 \leq y \leq -1, 0 \leq z \leq 2\}.$$

The measured wood occupies the domain

$$B = \left\{(x, y, z) | \, -3 \leq x \leq 3, -5 \leq y \leq 5, 3 \leq z \leq 5\right\}.$$

Moreover, we set the artificial boundaries to $[-10, 10] \times [-10, 10] \times [-10, 10]$. In the above domains, the unit of length is centimeters and the step size is $\alpha_x = \alpha_y = \alpha_z = \alpha = h_x = h_y = h_z = h = 1$. It is clear that the domain is symmetric. Based on the physical principles, $V_2 = -V_1$. Suppose $V_1 = 1$ and $V_2 = a$ (where a is an unknown to be determined). If, through numerical computation, the value of a is close to -1, it indicates that the multiple varying bounds integral method is reasonable.

We perform numerical experiments on the above example and obtain the data in Table 1. These data are consistent with the physical principle that C increases as ε increases. Based on the data, the corresponding image is shown in Figure 14(a). It can be seen that, compared with other methods [30], our method eliminates the initial oscillations and maintains the original trend of C variation. Figure 14(b) shows the fitted function image derived from Reference [30]. Then, we perform a regression analysis on these data to establish a regression model:

$$\varepsilon = 1.45C^2 - 97.31C + 1635.10. \tag{4.85}$$

Table 1. The numerical results of C about ε.

Dielectric constant ε	Capacitance value C	V_2
1	33.2245	-1.0458
2	33.8890	-1.0088
3	34.3597	-0.9900
4	34.7295	-1.0288
5	35.0345	-1.0198
6	35.2935	-1.0147
7	35.5178	-1.0112
8	35.7151	-1.0087
9	35.8906	-1.0067
10	36.0483	-1.0051
11	36.1910	-1.0039
12	36.3212	-1.0028
13	36.4407	-1.0019
14	36.5508	-1.0011
15	36.6528	-1.0050
16	36.7477	-0.9999
17	36.8363	-0.9994
18	36.9194	-0.9989
19	36.9974	-0.9985
20	37.0709	-0.9981

First, we evaluate the goodness of fit for Eq (4.85). A higher goodness of fit indicates a stronger ability of the model to predict the dependent variable. As calculated from the data presented in Table 2, the determination coefficient $R^2 = \frac{SSR}{SST} = \frac{603.42}{665} = 0.91$, where SSR represents the sum of squares regression and SST denotes the sum of squares total for Eq (4.85). This indicates that, when C is given, the regression model can more accurately predict the value of ε.

In addition, we consider the confidence degree, which represents the reliability of ε. The higher the confidence degree, the stronger the reliability. Table 2 shows that $F(1, 18) = 176.39$, and according to the F-distribution table, $F(1, 18) = 8.29$ ($\alpha = 0.01$). Because $176.39 > 8.29$, it can be concluded that the confidence degree of the model is greater than 0.99. This means the values of ε obtained through (4.85) are highly reliable and more concentrated around the true value. The results of this regression analysis indicate that the functional relationship model between ε and C that we established can effectively predict the value of ε from C, with small errors. It can be seen that the multiple varying bounds integral method is a valid numerical method for this kind of problem.

Table 2. The analysis of variance of regression model between C and ε.

Model	df	Sum of variance	MS	F	Significance F
Regression	1	603.42	603.42	176.39	9.69×10^{-11}
Residual	18	61.58	3.42		
Total	19	665			

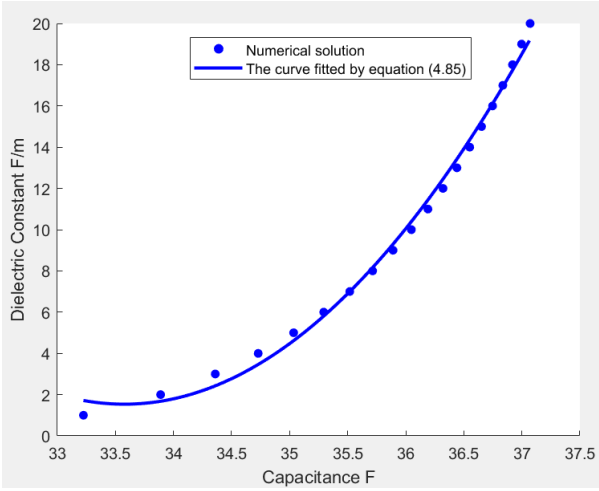

(a) Multiple varying bounds integral method.

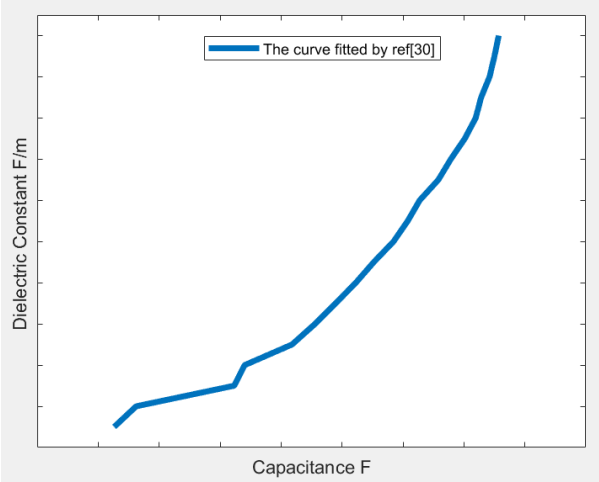

(b) Previous method in Reference [30].

Figure 14. The function image of C about ε.

5. Conclusions

Wood moisture content detection is an inverse problem in multi-physics fields. Based on the high precision demand for moisture content detection, we propose a new numerical method, that is, the multiple varying bounds integral method. Moreover, in different physics fields, we choose different discrete methods to construct numerical schemes. For the physical field where the unknown function is discontinuous, this field has to be divided into several additional parts. For each smaller part, such as faces, vertices, and edges, we build corresponding interpolation functions and handle the integral to meet the precision requirements for the engineering problem. Moreover, we carry out numerical experiments and perform regression analysis to obtain the function relationship between ε and C. This model obeys the physical principle that C increases with an increase in ε. Moreover, the established regression model R^2 is greater than 0.91, indicating a high goodness of fit and effectively reflecting

the relationship between ε and C. This demonstrates that the data derived from this method are valid. Additionally, this numerical method is applicable to other engineering problems.

On the other hand, the discrete scheme constructed in this paper has second-order precision. There are 2982 unknowns, and the computation time is 875.57 s. If a higher precision is desired, we can consider adding interpolation nodes to improve precision. Moreover, this would also increase the computational cost.

Use of AI tools declaration

The authors declare they have not used Artificial Intelligence (AI) tools in the creation of this article.

Acknowledgments

The authors would like to thank all the references which arehelpful for this article and the valuable suggestions which are put out by experts andreaders. These have improved this paper greatly and made it perfect. This paper was supported by the National Natural Science Foundation of China (Grant No. NSFC11526064), the Fundamental Research Funds for the Central Universities (Grant No. 3072024XX2402), and Harbin Engineering University (Grant No. KYWZ220240710).

Conflict of interest

The authors declare there are no conflicts of interest.

References

1. M. Broda, S. F. Curling, M. Frankowski, The effect of the drying method on the cell wall structure and sorption properties of waterlogged archaeological wood, *Wood Sci. Technol.*, **55** (2021), 971–989. https://doi.org/10.1007/s00226-021-01294-6
2. Z. B. He, J. Qian, L. J. Qu, Z. Y. Wang, S. L. Yi, Simulation of moisture transfer during wood vacuum drying, *Results Phys.*, **12** (2019), 1299–1303. https://doi.org/10.1016/j.rinp.2019.01.017
3. O. E. Özkan, Effects of cryogenic temperature on some mechanical properties of beech (Fagus orientalis Lipsky) wood, *Eur. J. Wood Wood Prod.*, **79** (2021), 417–421. https://doi.org/10.1007/s00107-020-01639-1
4. L. Rostom, S. Caré, D. Courtier-Murias, Analysis of water content in wood material through 1D and 2D H-1 NMR relaxometry: Application to the determination of the dry mass of wood, *Magn. Reson. Chem.*, **59** (2021), 614–627. https://doi.org/10.1002/mrc.5125
5. M. D. Ji, C. S. Gui, J. W. Ao, Y. F. Shen, J. Z. Zhao, J. J. Fu, Analysis of innovation trends of Chinese wood flooring industry (in Chinese), *China Wood-Based Panels*, **28** (2021), 7–9.
6. M. Li, D. Chen, K. Tian, J. M. He, Y. H. She, Experimental study on cracking load of wood membersunder different moisture content (in Chinese), *For. Eng.*, **38** (2022), 69–81.
7. X. Xu, H. Chen, B. H. Fei, W. F. Zhang, T. H. Zhong, Effects of age, particle size and moisture content on physical and mechanical properties of moso bamboo non-glue bonded composites (in Chinese), *J. For. Eng.*, **8** (2023), 30–37. https://doi.org/10.13360/j.issn.2096-1359.202204036

8. P. Dietsch, S. Franke, B. Franke, A. Gamper, S. Winter, Methods to determine wood moisture content and their applicability in monitoring concepts, *J. Civ. Struct. Health Monit.*, **5** (2015), 115–127. https://doi.org/10.1007/s13349-014-0082-7

9. L. Martin, H. Cochard, S. Mayr, E. Badel, Using electrical resistivity tomography to detect wetwood and estimate moisture content in silver fir, *Ann. For. Sci.*, **78** (2021), 65. https://doi.org/10.1007/s13595-021-01078-9

10. J. Van Blokland, S. Adamopoulos, Electrical resistance characteristics of thermally modified wood, *Eur. J. Wood Wood Prod.*, **80** (2022), 749–752. https://doi.org/10.1007/s00107-022-01813-7

11. W. R. N. Edwards, P. G. Jarvis, A method for measuring radial differences in water content of intact tree stems by attenuation of gamma radiation, *Plant Cell Environ.*, **6** (1983), 255–260. https://doi.org/10.1111/1365-3040.ep11587650

12. A. V. Batranin, S. L. Bondarenko, M. A. Kazaryan, A. A. Krasnykh, I. A. Miloichikova, S. V. Smirnov, et al., Evaluation of the effect of moisture content in the wood sample structure on the quality of tomographic X-Ray studies of tree rings of stem wood, *Bull. Lebedev Phys. Inst.*, **46** (2019), 16–18. https://doi.org/10.3103/S1068335619010056

13. P. A. Penttilä, M. Altgen, N. Carl, P. van Der Linden, I. Morfin, M. Österberg, et al., Moisture-related changes in the nanostructure of woods studied with X-ray and neutron scattering, *Cellulose*, **27** (2020), 71–87. https://doi.org/10.1007/s10570-019-02781-7

14. R. X. Qin, H. D. Xu, N. Z. Chen, Z. L. Zhen, J. D. Wei, The correlation between wood moisture content and dielectric constant based on dielectric spectroscopy (in Chinese), *J. Cent. South Univ. For. Technol.*, **42** (2022), 162–169. https://doi.org/10.14067/j.cnki.1673-923x.2022.03.017

15. W. Y. Tang, X. L. Zhang, *Sensors*, 6th edition, China Machine Press, Beijing, 2021.

16. V. T. H. Tham, T. Inagaki, S. Tsuchikawa, A new approach based on a combination of capacitance and near-infrared spectroscopy for estimating the moisture content of timber, *Wood Sci. Technol.*, **53** (2019), 579–599. https://doi.org/10.1007/s00226-019-01077-0

17. S. K. Korkua, S. Sakphrom, Low-cost capacitive sensor for detecting palm-wood moisture content in real-time, *Heliyon*, **6** (2020), e04555. https://doi.org/10.1016/j.heliyon.2020.e04555

18. H. Li, M. Perrin, F. Eyma, X. Jacob, V. Gibiat, Moisture content monitoring in glulam structures by embedded sensors via electrical methods, *Wood Sci. Technol.*, **52** (2018), 733–752. https://doi.org/10.1007/s00226-018-0989-y

19. Z. Wang, X. M. Wang, Z. J. Chen, Water states and migration in Xinjiang poplar and Mongolian Scotch pine monitored by TD-NMR during drying, *Holzforschung*, **72** (2018), 113–123. https://doi.org/10.1515/hf-2017-0033

20. D. Wu, *Several Studies on Finite Volume Methods for Diffusion Problems (in Chinese)*, Ph.D thesis, Jilin University, 2023.

21. X. Liu, *Research on Polyhedral Mesh Quality Based on Finite Volumn Method (in Chinese)*, Ph.D thesis, Chongqing University of Posts and Telecommunications, 2022. https://doi.org/10.27675/d.cnki.gcydx.2022.001125

22. U. Ahmed, D. S. Mashat, D. A. Maturi, Finite volume method for a time-dependent convection-diffusion-reaction equation with small parameters, *Int. J. Differ. Equations*, **2022** (2022), 3476309. https://doi.org/10.1155/2022/3476309

23. Y. S. Luo, X. L. Li, C. Guo, Fourth-order compact and energy conservative scheme for solving nonlinear Klein-Gordon equation, *Numer. Methods Partial Differ. Equations*, **33** (2017), 1283–1304. https://doi.org/10.1002/num.22143

24. C. Guo, W. J. Xue, Y. L. Wang, Z. X. Zhang, A new implicit nonlinear discrete scheme for Rosenau-Burgers equation based on multiple integral finite volume method, *AIP Adv.*, **10** (2020), 045125. https://doi.org/10.1063/1.5142004

25. C. Guo, F. Li, W. Zhang, Y. S. Luo, A conservative numerical scheme for rosenau-rlw equation based on multiple integral finite volume method, *Bound. Value Probl.*, **2019** (2019), 168. https://doi.org/10.1186/s13661-019-1273-2

26. C. Guo, Y. Wang, Y. S. Luo, A conservative and implicit second-order nonlinear numerical scheme for the rosenau-kdv equation, *Mathematics*, **9** (2021), 1183. https://doi.org/10.3390/math9111183

27. J. N. Wu, C. Guo, B. Y. Fan, X. B. Zheng, X. L. Li, Y. X. Wang, Two high-precision compact schemes for the dissipative symmetric regular long wave (SRLW) equation by multiple varying bounds integral method, *AIP Adv.*, **14** (2024), 125009. https://doi.org/10.1063/5.0233771

28. Y. S. Luo, C. Guo, Q. S. Liu, S. Liang, S. G. Liu, Mathematical model and its application of the planar capacitance sensor under non-uniform and non-symmetrical conditions (in Chinese), *Chin. J. Eng. Math.*, **30** (2013), 317–328.

29. D. Chalishajar, D. Kasinathan, R. Kasinathan, Viscoelastic Kelvin–Voigt model on Ulam–Hyer's stability and T-controllability for a coupled integro fractional stochastic systems with integral boundary conditions via integral contractors, *Chaos Solitons Fractals*, **191** (2025), 115785. https://doi.org/10.1016/j.chaos.2024.115785

30. C. Guo, *Research on Mathematical Model and Algorithm of Capacitance Sensor Used to Detect Wood Moisture Content (in Chinese)*, Ph.D thesis, Harbin Engineering University, 2014.

AIMS Press